Supplementary Data

Uranium (VI) Adsorbate Structures on Portlandite [$Ca(OH)_2$] Type Surfaces Determined by Computational Modelling and X-Ray Absorption Spectroscopy

Christopher A. Lee [1], Arjen van Veelen [2], Katherine Morris [3], J. Fred W. Mosselmans [4], Roy A. Wogelius [3,*] and Neil A. Burton [5,*]

1 National Nuclear Laboratory Limited, NNL, Abingdon, OX14 3DB Oxfordshire, UK; christopher.lee@uknnl.com
2 Material Science and Technology Division, Los Alamos National Laboratory, Los Alamos, NM 87545, USA ; arjen.vanveelen@lanl.gov
3 Department of Earth and Environmental Sciences, University of Manchester, M13 9PL Manchester, UK; katherine.morris@manchester.ac.uk
4 Department, Diamond Light Source, OX11 0DE Didcot, UK; fred.mosselmans@diamond.ac.uk
5 Department of Chemistry, University of Manchester, M13 9PL Manchester, UK;
* Correspondence: roy.wogelius@manchester.ac.uk (R.A.W.); neil.burton@manchester.ac.uk (N.A.B.)

Hydroxyl-water ligand exchange details.

Additional PMF simulations were performed to assess the hydroxyl-water ligand exchange energy corresponding to the following reactions:

$UO_2(OH)_n(H_2O)_{m-n} \rightarrow UO_2(OH)_{n-1}(H_2O)_{m+1-n} + OH^-$ (n = 3,4, and 5).

For $[UO_2(OH)_3]^-$ and $[UO_2(OH)_4]^{2-}$ the equatorial coordination number m=4, but this was not constrained in the simulations; for $[UO_2(OH)_5]^{3-}$ no additional water ligands were observed to coordinate to uranium. In these simulations, the collective variable being sampled was the distance between the uranium atom and the oxygen atom of the hydroxyl group being removed from the complex. The different uranyl hydroxide species were placed into a cubic simulation cell of side length 31 Å and solvated with 984 TIP4P/2005 water molecules, corresponding to a density of approximately 1 g cm^{-3}. Sampling of the collective variable was performed every ten timesteps and a cut off of 8.5 Å was used for the van der Waals interactions.

Analysis of the radial distribution functions for the $[UO_2(H_2O)(OH)_3]^-$ and $[UO_2(OH)_4]^{2-}$ complexes shows that the U-OH^- distance is 2.28 Å, and for the $[UO_2(OH)_5]^{3-}$ complex the U-OH^- distance is slightly longer at 2.33 Å. The U-water distance in the $[UO_2(H_2O)(OH)_3]^-$ complex is 2.63 Å. From a kinetic perspective, we note that the barrier to the first dissociation of OH^- from $[UO_2(OH)_5]^{3-}$ is approximately 38 kJ mol^{-1}. Subsequent dissociation of OH^-, with barriers of approximately 90 kJ mol^{-1} and 116 kJ mol^{-1}, result in exchange of hydroxyl by a water molecule. The backward barriers, corresponding to exchange of water by hydroxyl in $UO_2(H_2O)(OH)_3]^{3-}$ and $[UO_2(H_2O)_2(OH)_2]$ are considerably lower, ~34 and <5 kJ mol^{-1} respectively.

It should be noted that the relative energies are higher than those determined experimentally. Gibbs energies of formation for $UO_2(OH)_4^{2-}$ (aq), $UO_2(OH)_3^-$ (aq) and $UO_2(OH)_2$ (aq) have been determined from equilibrium data [52, 62] as –1716.2, –1548.3 and –1357.5 kJ mol^{-1} respectively. Combining with $G(OH^-,aq)$=–157.5 kJ mol^{-1} [72] would suggest $UO_2(OH)_3^-$ and $UO_2(OH)_2$ to be only 10 and 43 kJ mol^{-1} less stable respectively; no thermodynamic data is available for the $UO_2(OH)_5^{3-}$ complex. These discrepancies are perhaps a reflection on the limitations of the classical potentials which have not been optimised for these equilibria. The thermodynamics of these ligand exchange equilibria are largely driven by the solvation of the respective ions and errors of 10-15% with unoptimised classical potentials are not uncommon [73, 74]. For example, it can be seen that a systematic adjustment of around 11% (50 kJ mol^{-1}) to the effective solvation energy of the hydroxyl ion would bring the experimental and computational results into considerably better agreement, including the destabilisation of $[UO_2(OH)_5]^{3-}$ relative to the other species as

expected. The classical potentials employed in this work are non-polarizable and a compromise has been made to facilitiate the sorption studies such that bulk calcium hydroxyl parameters were used for both the uranyl hydroxyls in all simulations and the aqueous hydroxyl in the speciation equilibria. We also note our free energy values to be upper limits due to the difficulty converging the sampling of the PMFs as the fragments dissociate.

Preliminary PMF Adsorption Calculations

We first consider sorption of UO_2^{2+}, which would initially have charge compensated by 5 equatorial water molecules (see Figure S2). The UO_2^{2+} ion is able to burrow into the interlayer space of the (203/101) surface allowing the uranium atom to coordinate to four hydroxyl groups to give a large negative free energy change of –173 kJ mol^{-1}. Similar behaviour is displayed on the (100) surface, again with a large negative energy change of –64 kJ mol^{-1}. Burrowing does not occur on the (001), however adsorption is energetically favourable (-1.2 kJ mol^{-1}) at a distance from the surface of approximately 3 Å. UO_2^{2+} forms a stable bridged inner-sphere complex with the O=U=O parallel to the surface by exchange of equatorial water with 2 surface hydroxyl groups.

The PMF results for the second positive complex, $UO_2(OH)^+$ (with four initial water molecules), are shown in Figure S3. $UO_2(OH)^+$ bridges two exposed hydroxyl groups and extracts a third from the surface forming a bound $UO_2(OH)_4^{2-}$ complex on the (203/101) surface, giving a favourable free energy change of -43 kJ mol^{-1}. $UO_2(OH)^+$ adsorbs onto the (100) by bridging two surface hydroxyl groups, while a third hydroxyl shifts position such that it bridges two calcium atoms across the interlayer space and the uranium atom giving a free energy change of -20 kJ mol^{-1} . $UO_2(OH)^+$ forms a similar surface complex on the (001) surface to UO_2^{+2}, also with a favourable but small energy change of –3.3 kJ mol^{-1}.

Figure S4 shows the PMF results for $UO_2(OH)_2$ (with two initial water molecules). $UO_2(OH)_2$ also burrows into the (203/101) surface in a similar manner to the UO_2^{2+} ion with the uranium atom coordinating to three surface hydroxyl groups to complete a 4 coordinate structure resulting again in a large negative free energy of adsorption of –26 kJ mol^{-1}. On the (100) surface $UO_2(OH)_2$ adsorbs by dissociating a water ligand and coordinating to a surface hydroxyl group, which shifts the adsorbate out to ~3 Å and gives a small negative free energy change of –11 kJ mol^{-1}. Again, the adsorbate configuration on the (001) for $UO_2(OH)_2$ repeats the behaviour displayed by the previous two species, forming a stable parallel inner sphere complex with an energy change of -13 kJ mol^{-1}.

Pertinent only to the pH region well above those expected in a GDF, the even more hydroxylated species $UO_2(OH)_5^{3-}$ is considered on Figure S6. Adsorption is expected to be minimal for this species onto portlandite. On the (100) surface $UO_2(OH)_5^{3-}$ dissociates a hydroxyl group to the surface which bridges two calcium atoms to provide weak distal possible attachment. As with the previous species adsorption onto the (001) is unfavourable. The $UO_2(OH)_5^{3-}$ complex adsorbs onto the (203/101) surface in such a way as to partially displace a surface hydroxyl away from one of its calcium ions, two of the complex hydroxyl groups then bridge this calcium atom and an adjacent calcium atom, however the free energy change is minimal.

References

72. Klaning, U.K.; Sehested, K.; Holcman, J. Standard Gibbs energy of formation of the hydroxyl radical in aqueous solution—Rate constants for the reaction $ClO_2^- + O_3 \leftrightarrow O_3^- + ClO_2$. *J. Phys. Chem.* **1985**, *89*, 760–763.

73. Joung, I.S.; Cheatham, T.E. Determination of alkali and halide monovalent ion parameters for use in explicitly solvated biomolecular simulations. *J. Phys. Chem. B* **2008**, *112*, 9020–9041.

74. Lee, M.W.; Meuwly, M. Hydration free energies of cyanide and hydroxide ions from molecular dynamics simulations with accurate force fields. *Phys. Chem. Chem. Phys.* **2013**, *15*, 20303–20312.

75. Momma, K.; Izumi, F. VESTA 3 for three-dimensional visualization of crystal, volumetric and morphology data. *J. Appl. Crystallogr.* **2011**, *44*, 1272–1276.

76. Moll, H.; Rossberg, A.; Steudtner, R.; Drobot, B.; Mueller, K.; Tsushima, S. Uranium(VI) chemistry in strong alkaline solution: Speciation and oxygen exchange mechanism. *Inorg. Chem.* **2014**, *53*, 1585–1593.

Coordinates

CIF files are available for the optimised ⊥ and ∥ (001),(100),(203/101),(001-OH),(100-OH) and (203-OH) structures at the DFT level on request.

Table S1. Gas phase surface energies.

Surface	Surface Energy (J m^{-2})	
	Classical MD (T = 298 K)	DFT (T = 0 K)
(001)	0.11	0.06
(100)	0.86	0.45
(203)	0.60	0.36

Table S2. Portlandite lattice parameters (= = 90 and =120).

	a (Å)	c (Å)
Classical	3.662 (2.03%)	4.740 (−3.48%)
DFT (PBE)	3.644 (1.53%)	4.993 (1.67%)
Experimental [2]	3.589	4.911

Table S3. U(VI) substituted lattice parameters (5 × 5 × 5 supercell).

	a (Å)	c (Å)
Pure Portlandite	18.218 (1.52%)	24.963 (1.66%)
U(VI) substituted Portlandite	18.171 (1.26%)	24.561 (0.24%)
UO_2 substituted Portlandite	18.189 (1.36%)	24.700 (0.59%)
Experimental	17.945	24.555

(101)

[a]

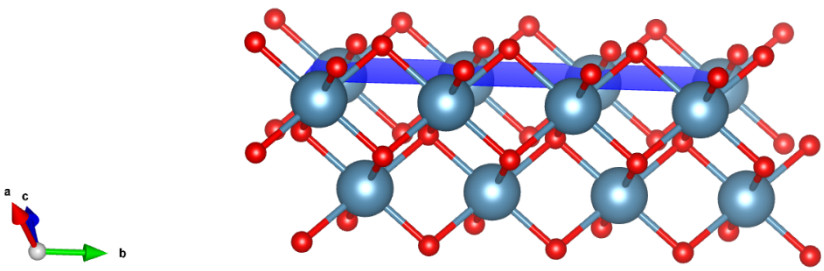

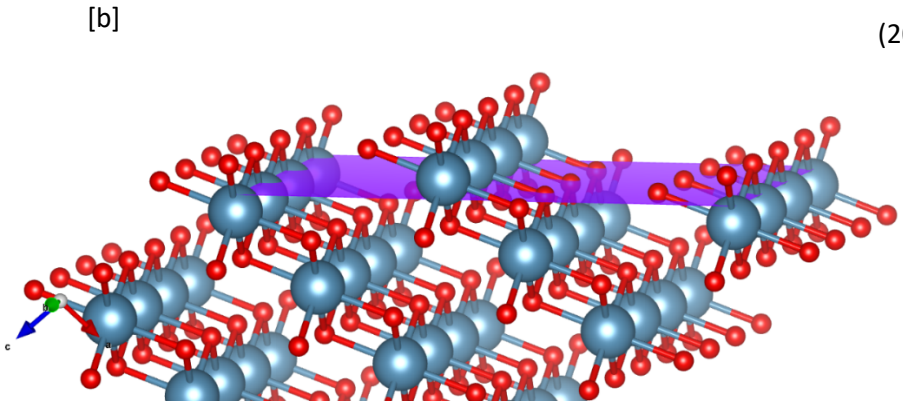

Figure S1. Comparison of the [a] (101) [blue transparent plane] and [b] (203) [purple transparent plane] surfaces of portlandite, showing the step difference between the two (Ca = grey, OH = red). Drawn using Vesta 3 [75].

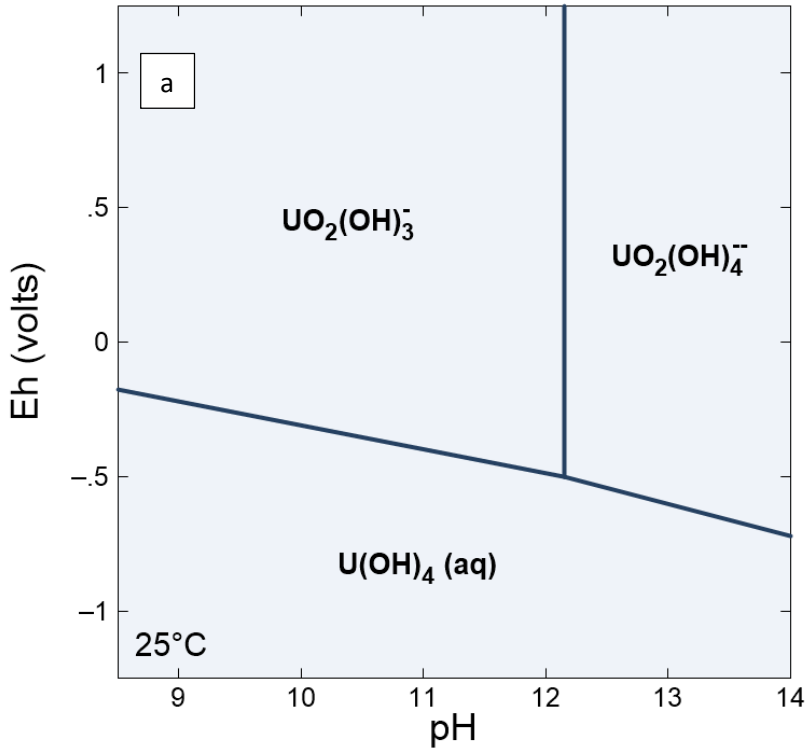

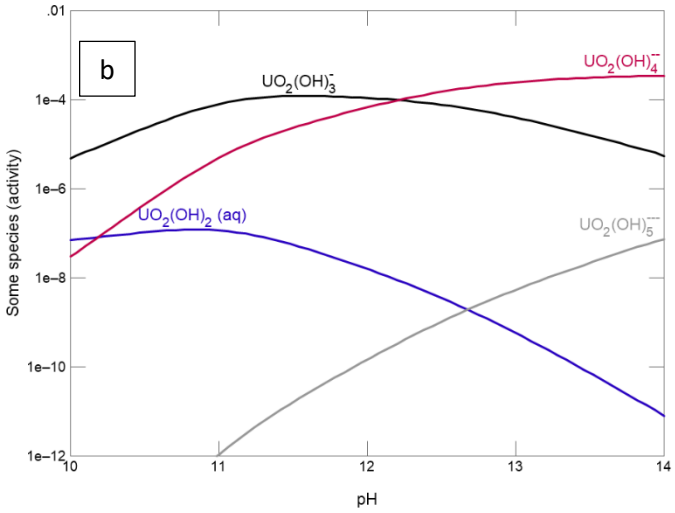

Figure S2. (**a**) Uranyl speciation using MINTEQ database. Note the predominance of $UO_2(OH)_4^{--}$ above pH ~12. (**b**) Uranyl species predominance for a 25 ppm uranyl solution, again calculated using the MINTEQ database but showing an estimated activity for UO2(OH)5--- in the pH range of interest (estimated from the G values in [76]) showing that the pentahydroxyl species is most probably negligible in the range pH 12 to 13.

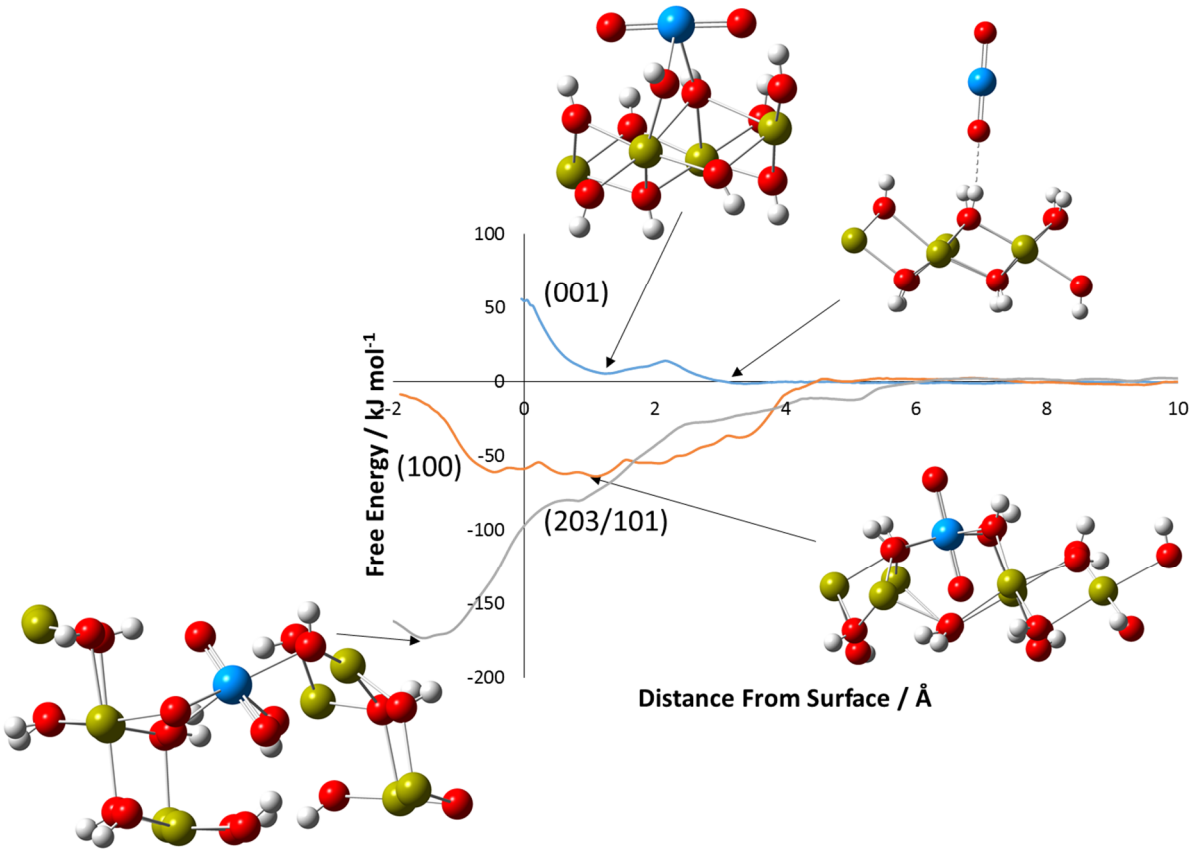

Figure S3. PMF (free energy) plots for the sorption of UO_2^{2+} to the (001), (100) and (203/101) surfaces of portlandite.

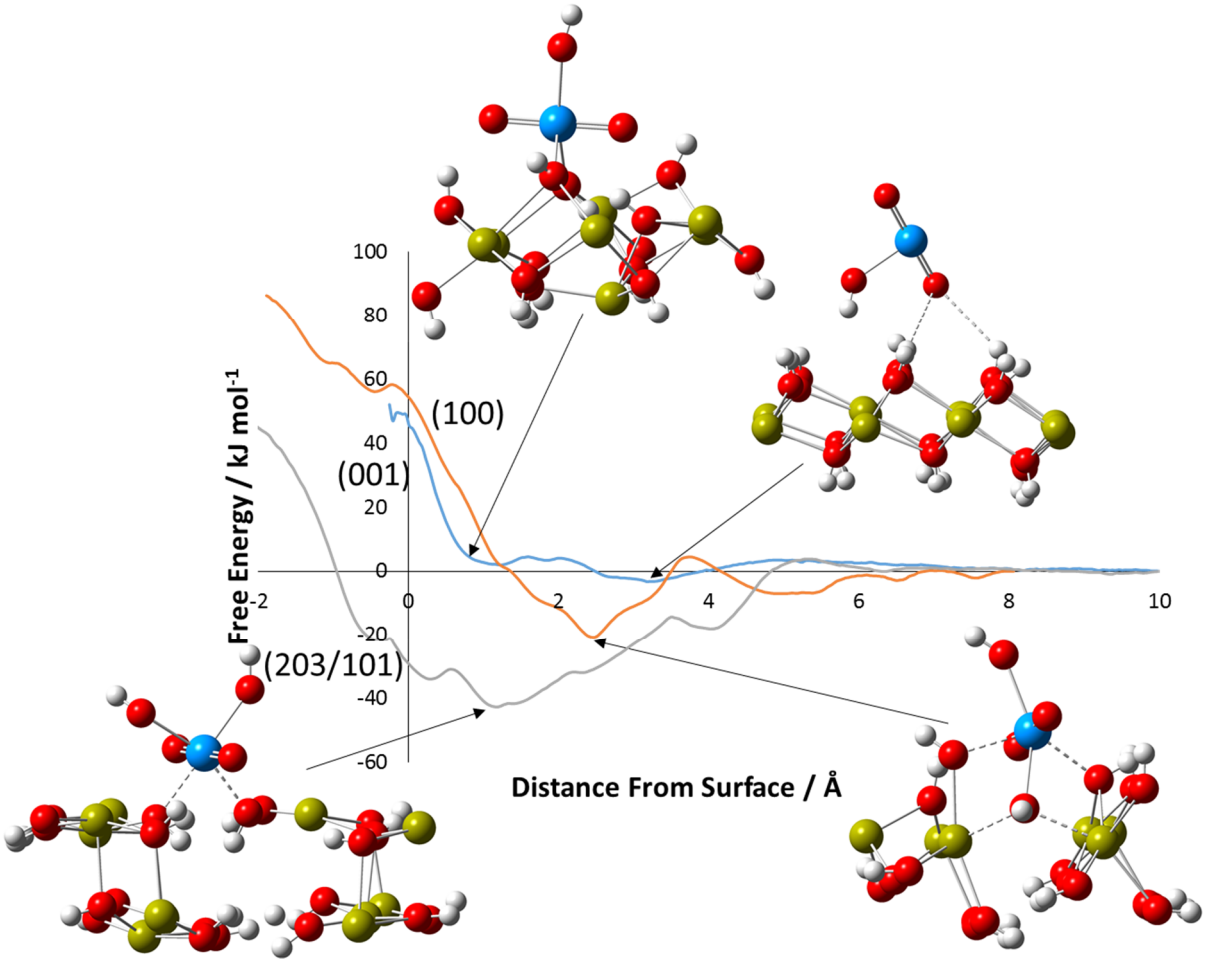

Figure S4. PMF (free energy) plots for the sorption of $[UO_2(OH)]^+$ to the (001), (100) and (203/101) surfaces of portlandite.

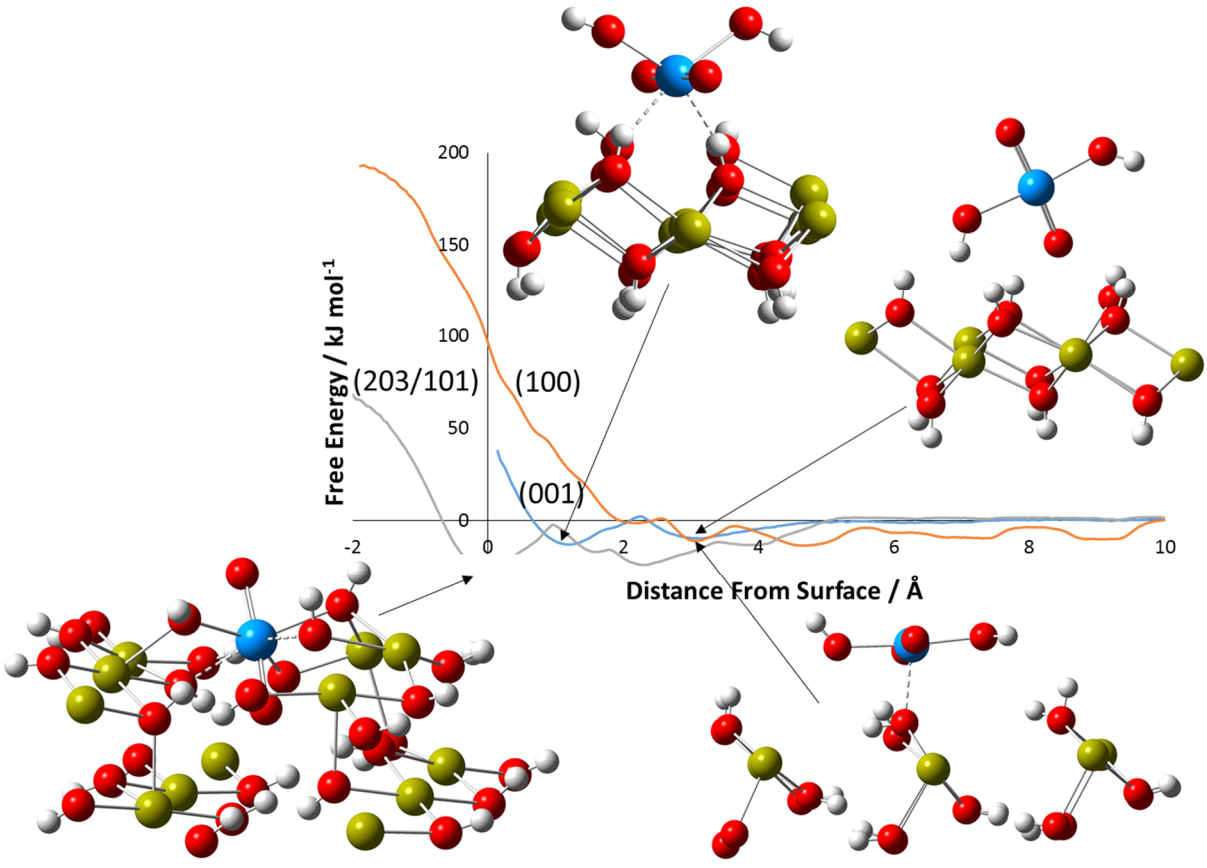

Figure S5. PMF (free energy) plots for the sorption of $[UO_2(OH)_2]$ to the (001), (100) and (203/101) surfaces of portlandite.

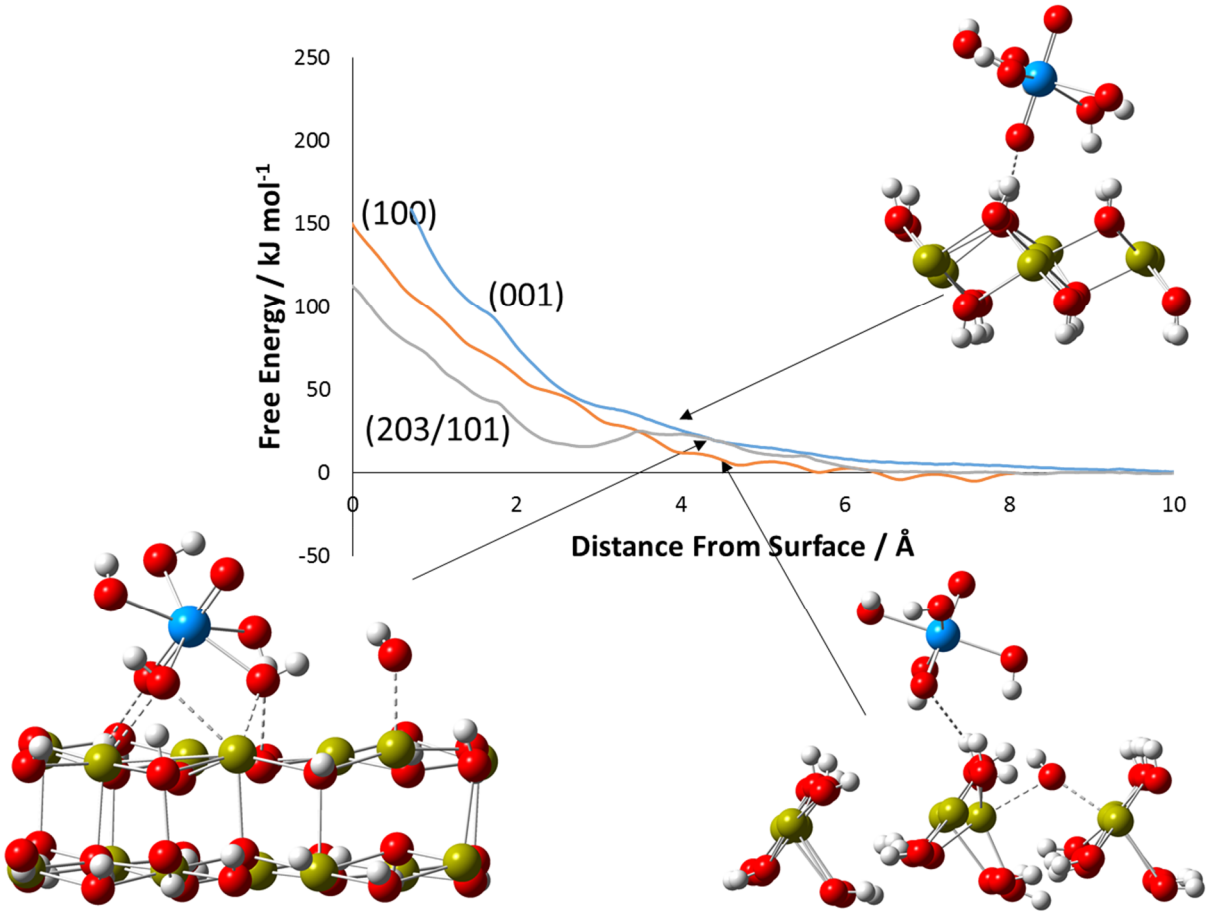

Figure S6. PMF (free energy) plots for the sorption of $[UO_2(OH)_5]^{3-}$ to the (001), (100) and (203/101) surfaces of portlandite.

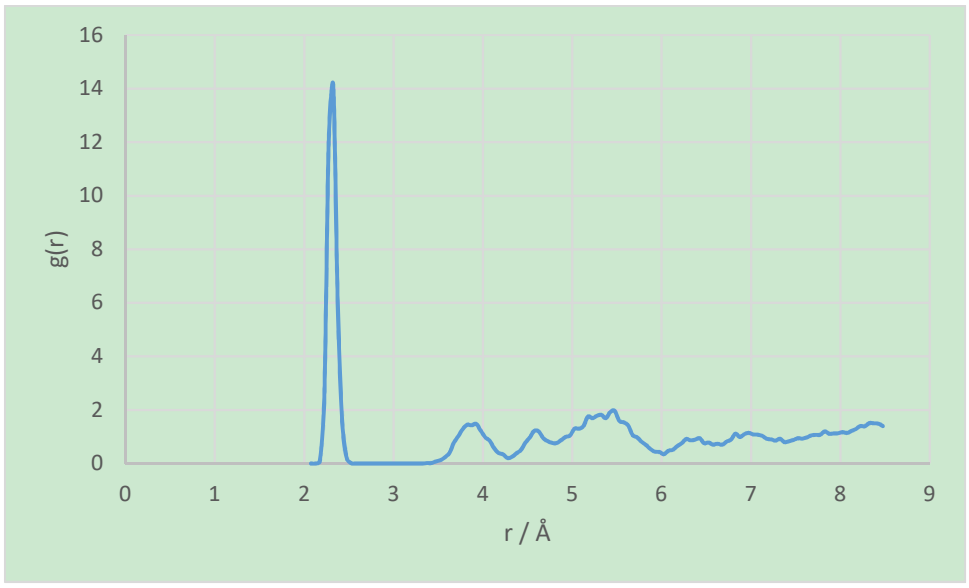

Figure S7. U-Oh RDF for the UO_2^{2+} bridging structure on the (001) surface of portlandite.

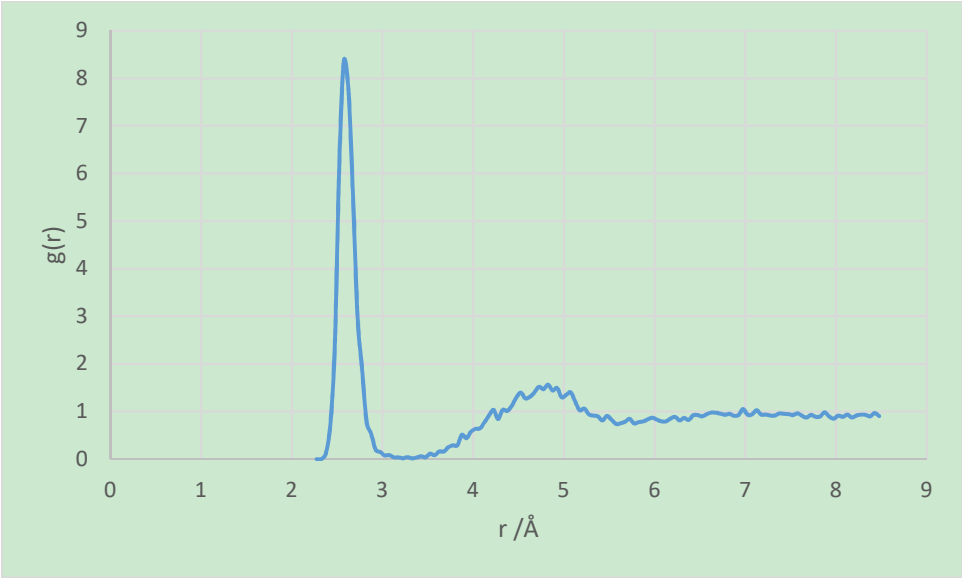

Figure S8. U-Ow RDF for the UO_2^{2+} bridging structure on the (001) surface of portlandite.

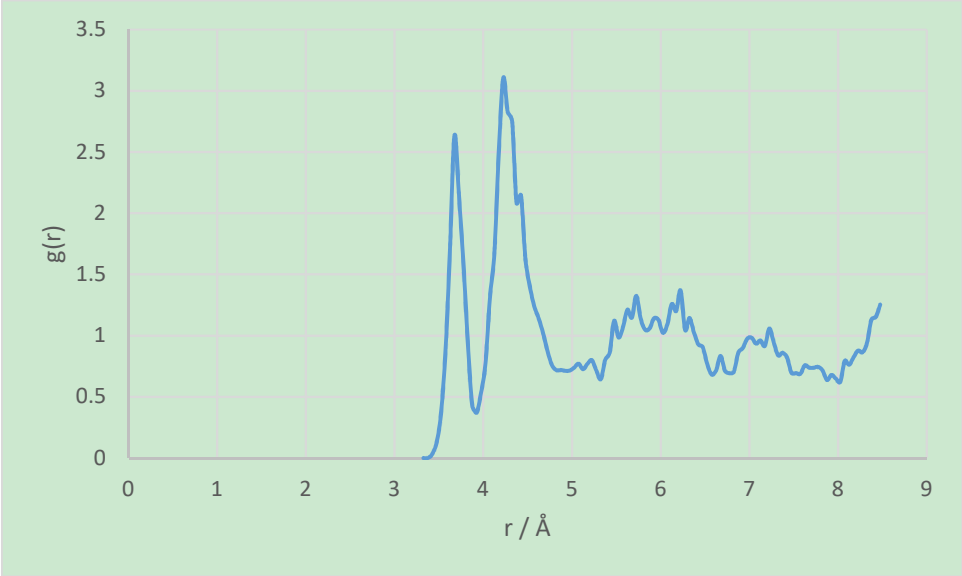

Figure S9. U-Ca RDF for the UO_2^{2+} bridging structure on the (001) surface of portlandite.

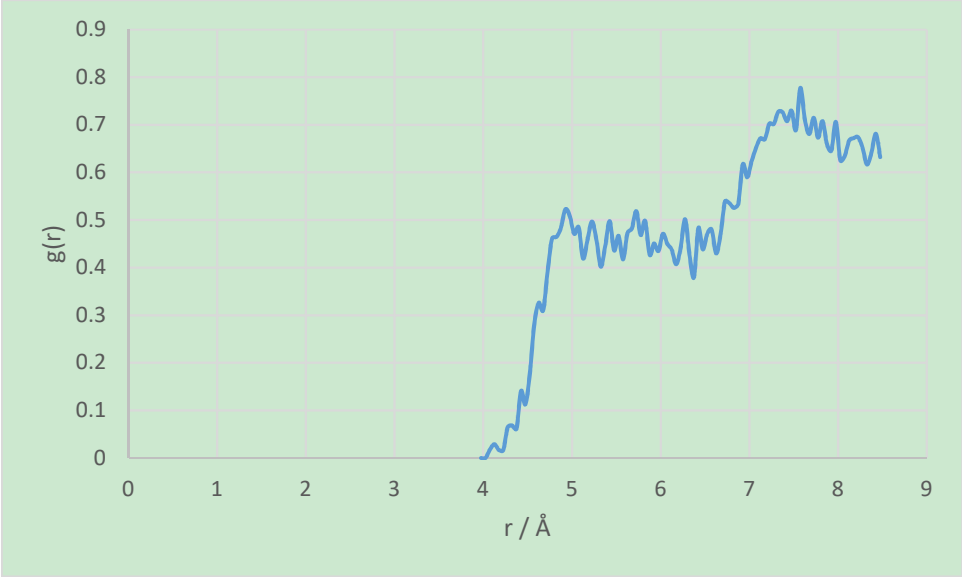

Figure S10. U-Oh RDF for UO_2^{2+} on the (001) surface of portlandite.

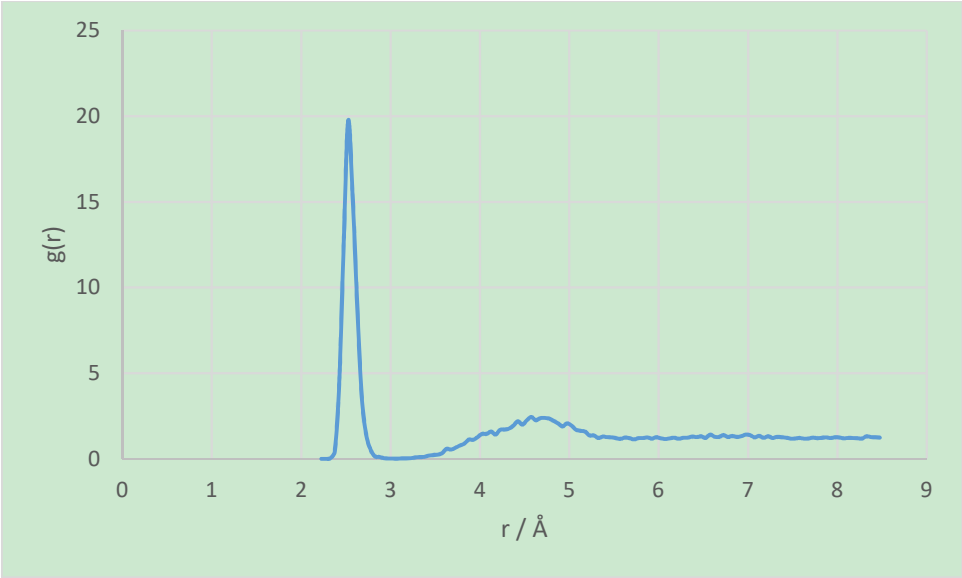

Figure S11. U-Ow RDF for UO_2^{2+} on the (001) surface of portlandite.

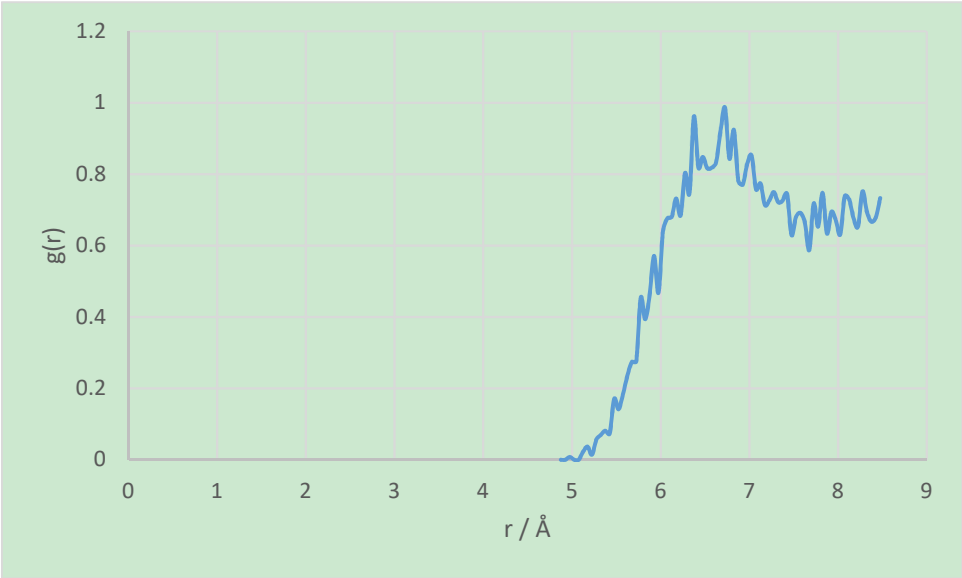

Figure S12. U-Ca RDF for UO_2^{2+} on the (001) surface of portlandite.

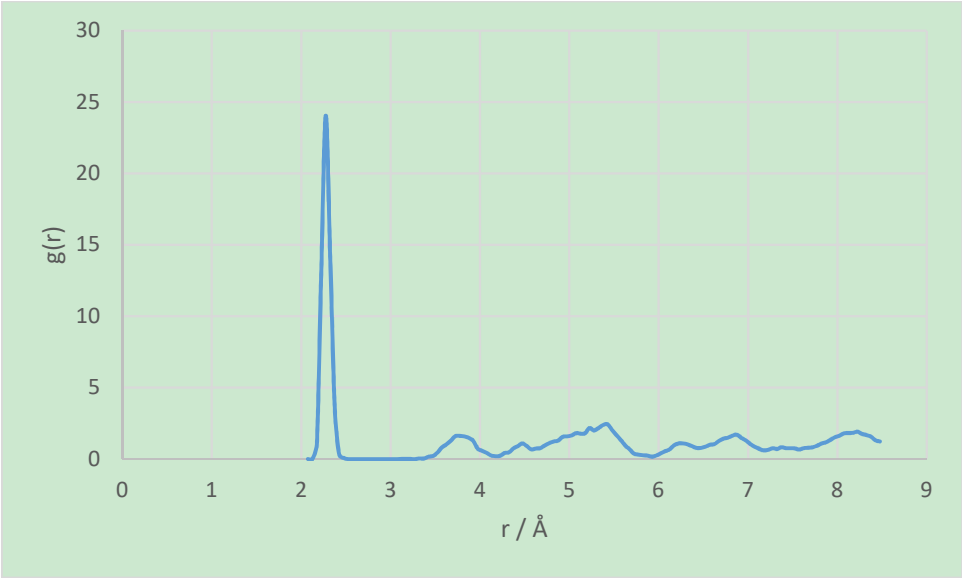

Figure S13. U-Oh RDF for the $UO_2(OH)^+$ bridging structure on the (001) surface of portlandite.

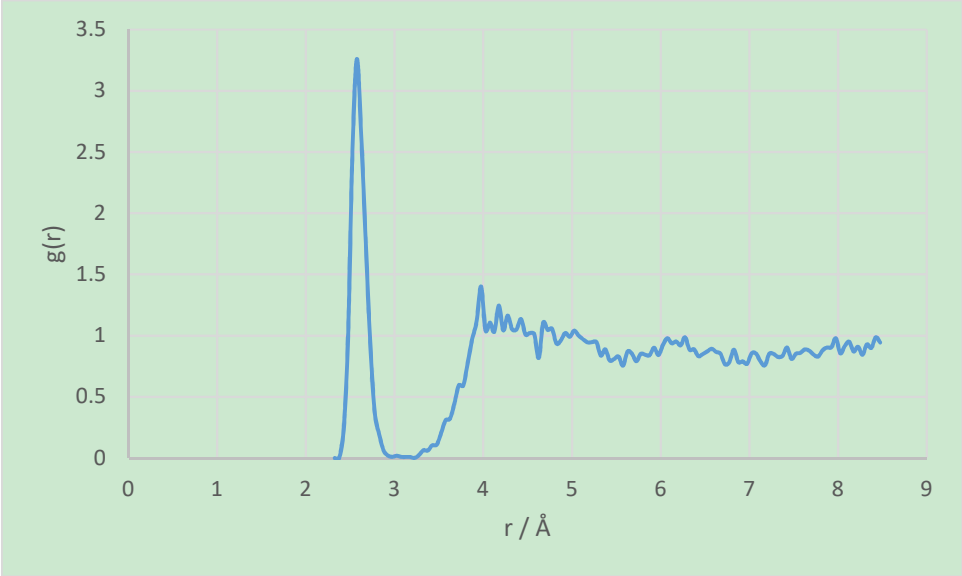

Figure S14. U-Ow RDF for the $UO_2(OH)^+$ bridging structure on the (001) surface of portlandite.

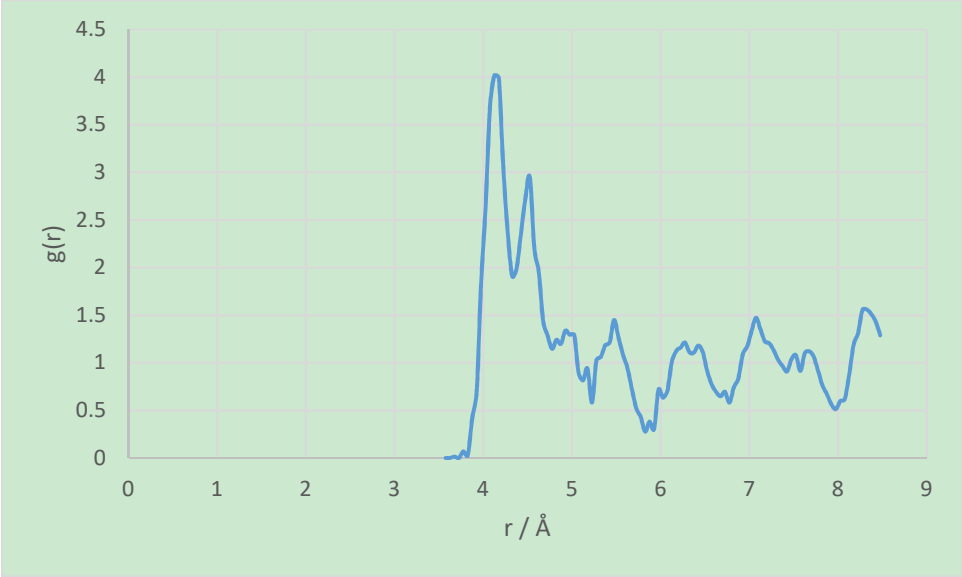

Figure S15. U-Ca RDF for the $UO_2(OH)^+$ bridging structure on the (001) surface of portlandite.

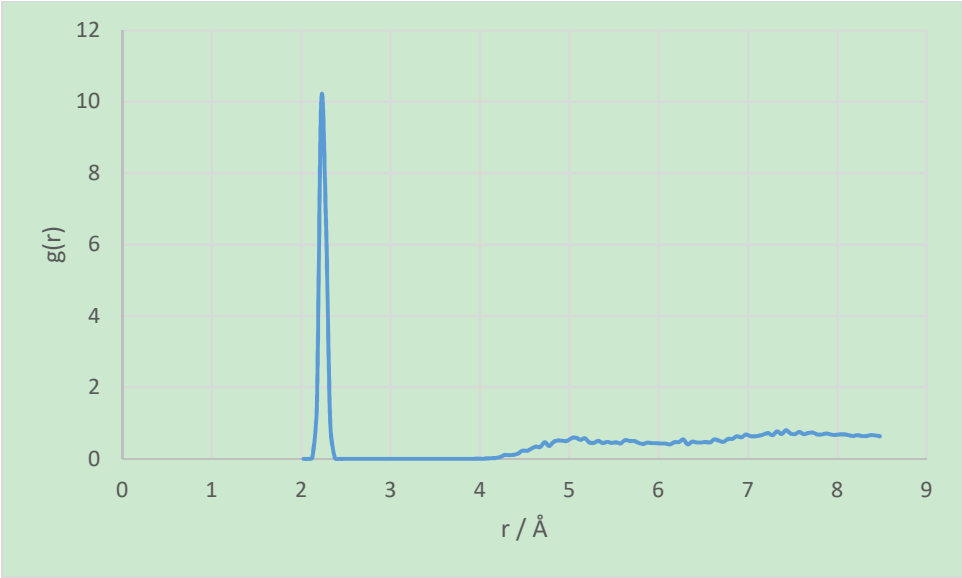

Figure S16. U-Oh RDF for $UO_2(OH)^+$ on the (001) surface of portlandite.

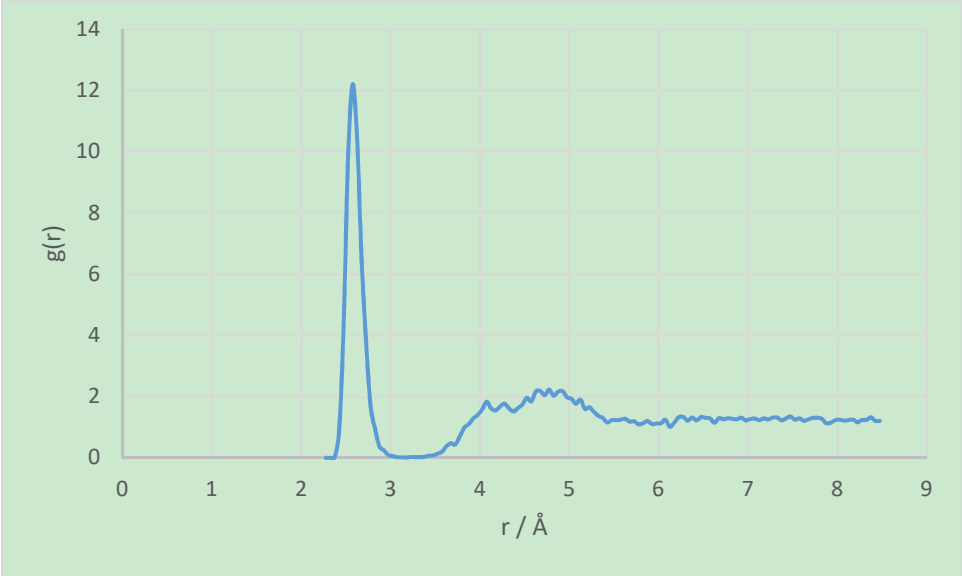

Figure S17. U-Ow RDF for $UO_2(OH)^+$ on the (001) surface of portlandite.

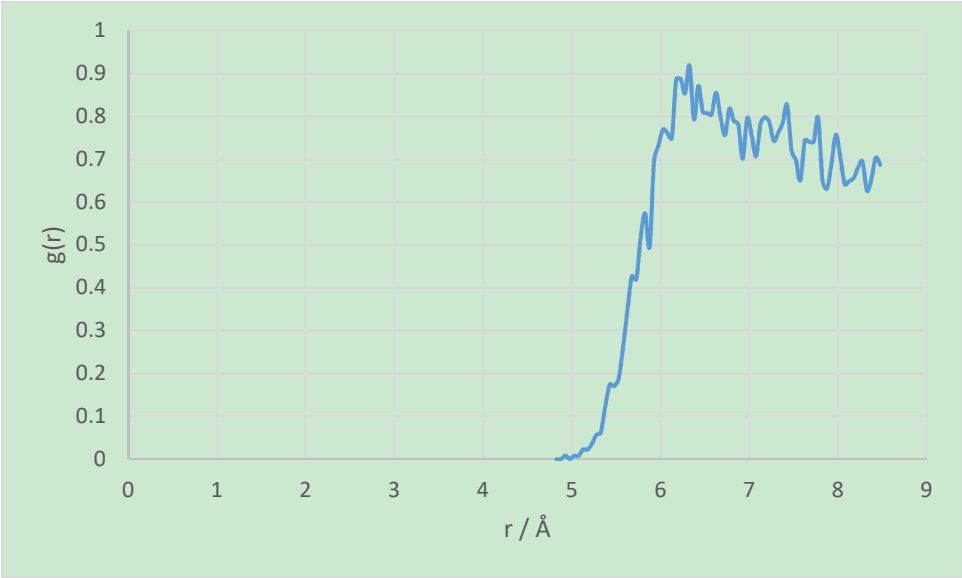

Figure S18. U-Ca RDF for $UO_2(OH)^+$ on the (001) surface of portlandite.

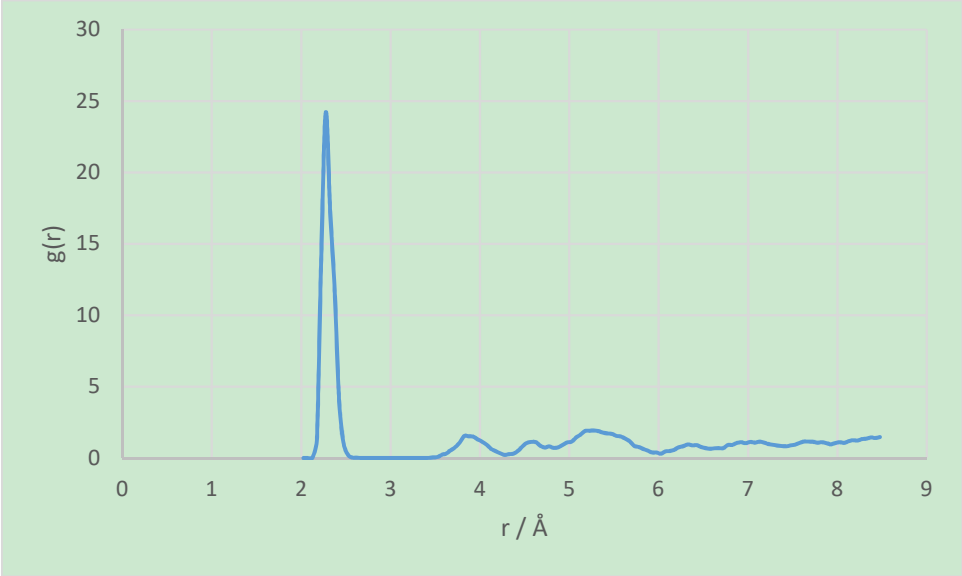

Figure S19. U-Oh RDF for the $UO_2(OH)_2$ bridging structure on the (001) surface of portlandite.

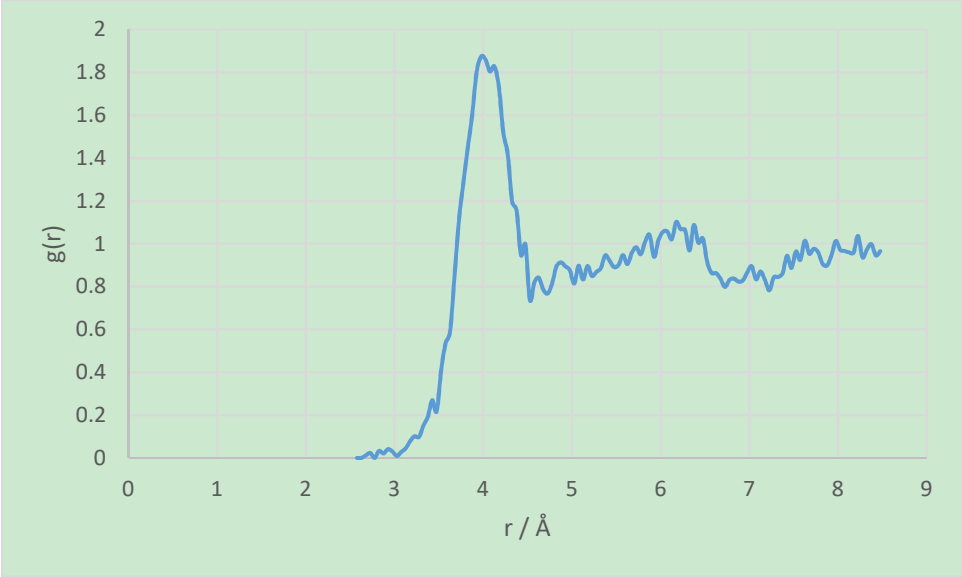

Figure S20. U-Ow RDF for the $UO_2(OH)_2$ bridging structure on the (001) surface of portlandite.

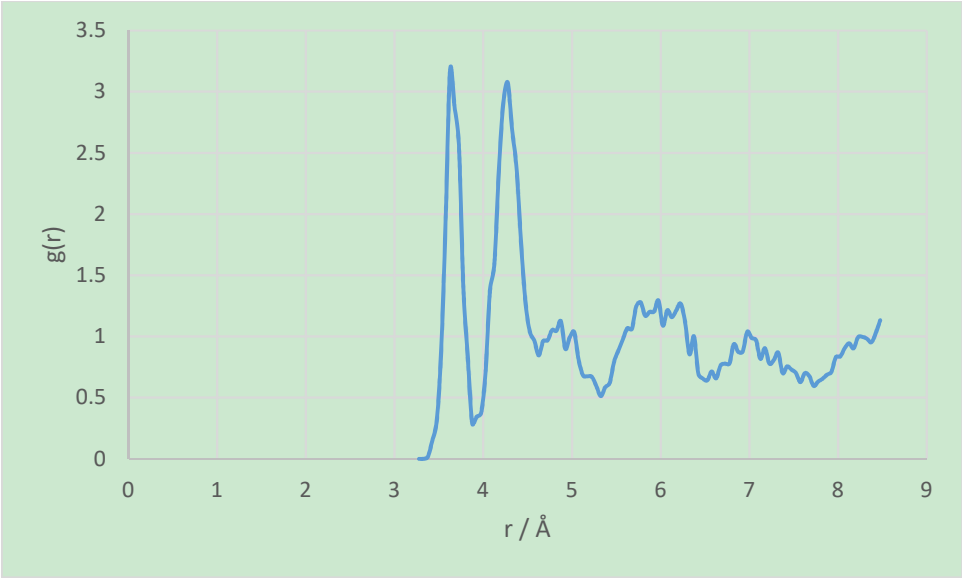

Figure S21. U-Ca RDF for the $UO_2(OH)_2$ bridging structure on the (001) surface of portlandite.

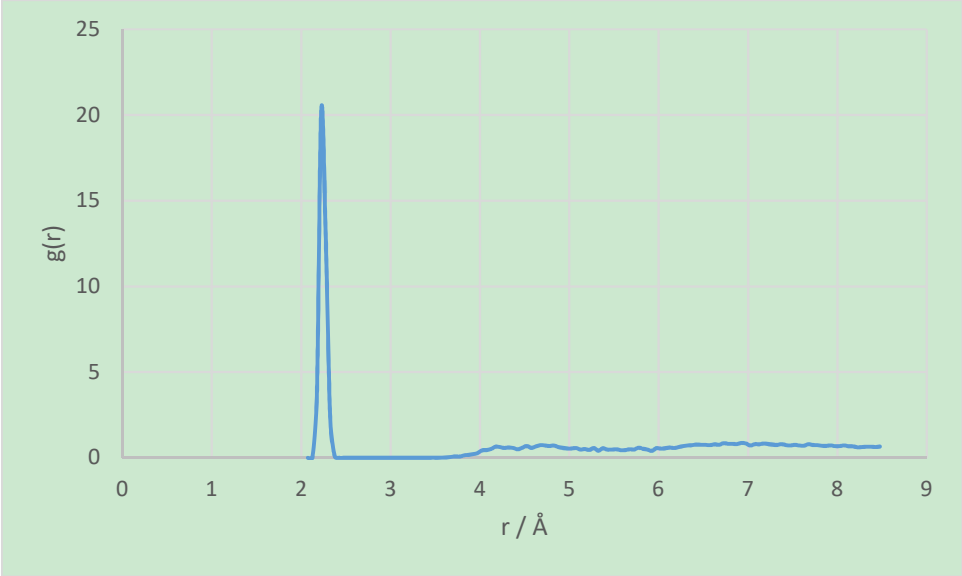

Figure S22. U-Oh RDF for $UO_2(OH)_2$ on the (001) surface of portlandite.

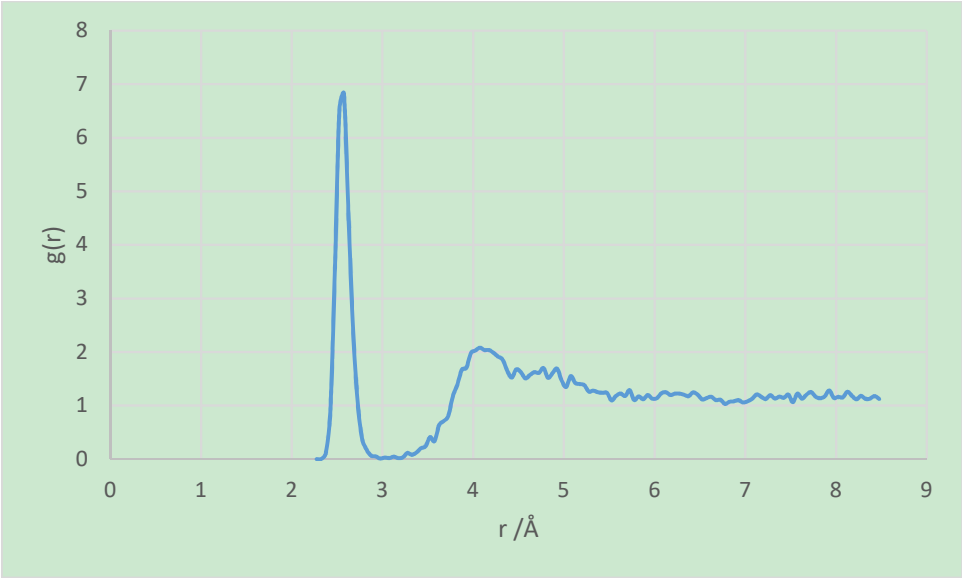

Figure S23. U-Ow RDF for $UO_2(OH)_2$ on the (001) surface of portlandite.

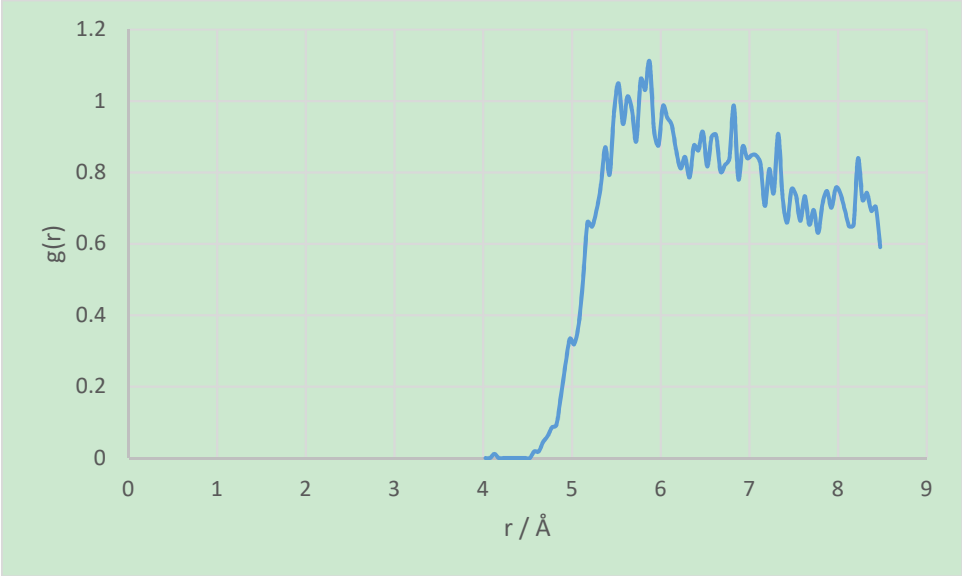

Figure S24. U-Ca RDF for $UO_2(OH)_2$ on the (001) surface of portlandite.

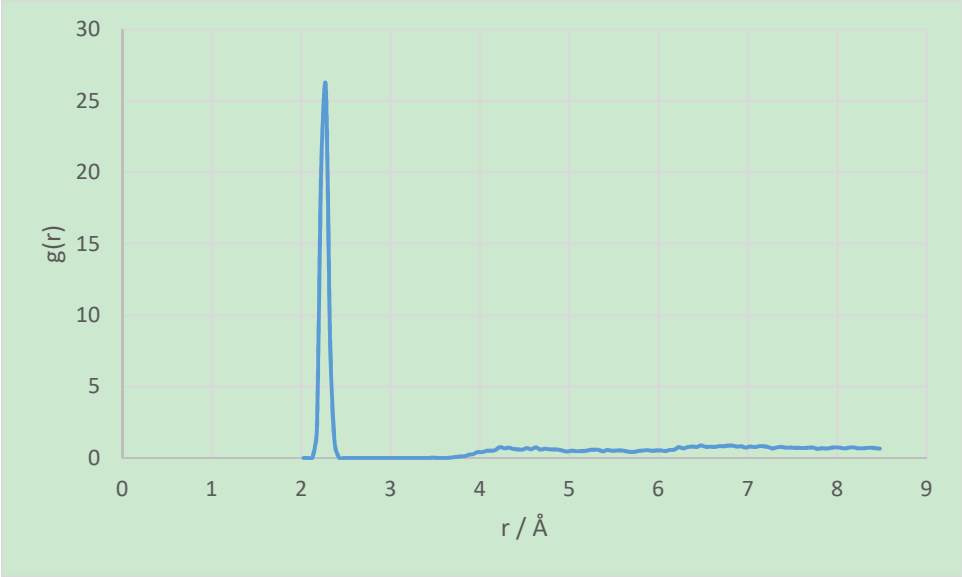

Figure S25. U-Oh RDF for $UO_2(OH)_3^-$ on the (001) surface of portlandite.

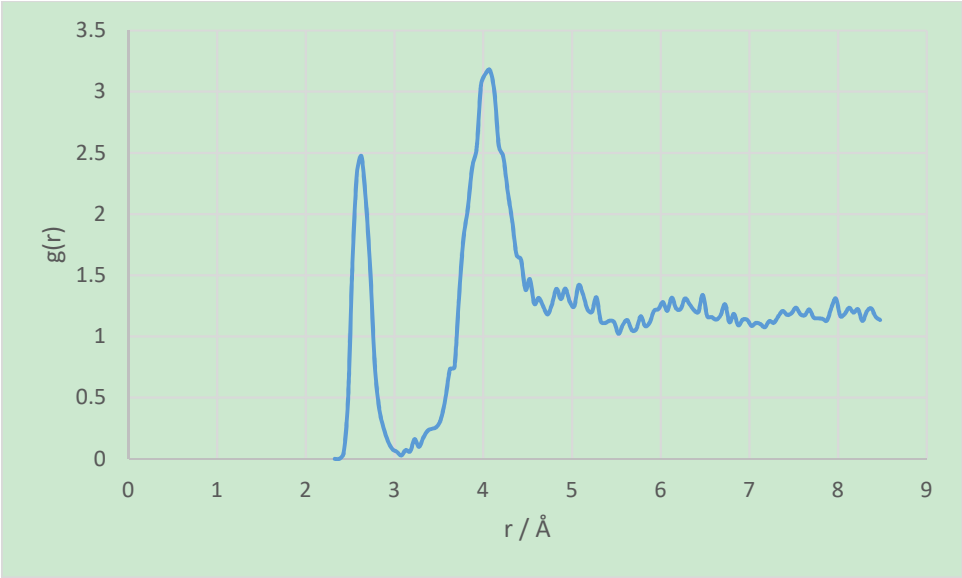

Figure S26. U-Ow RDF for $UO_2(OH)_3^-$ on the (001) surface of portlandite.

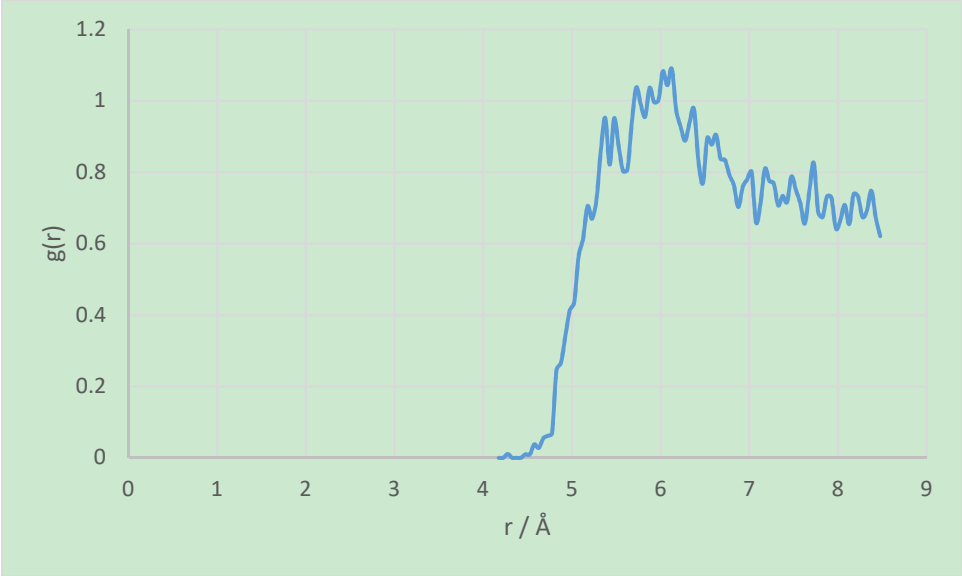

Figure S27. U-Ca RDF for $UO_2(OH)_3^-$ on the (001) surface of portlandite.

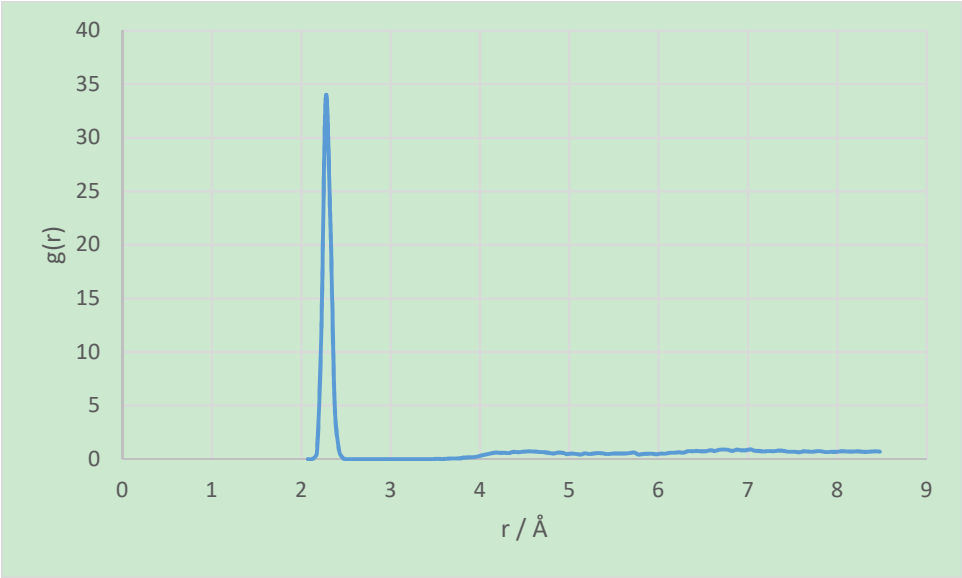

Figure S28. U-Oh RDF for $UO_2(OH)_4^{2-}$ on the (001) surface of portlandite.

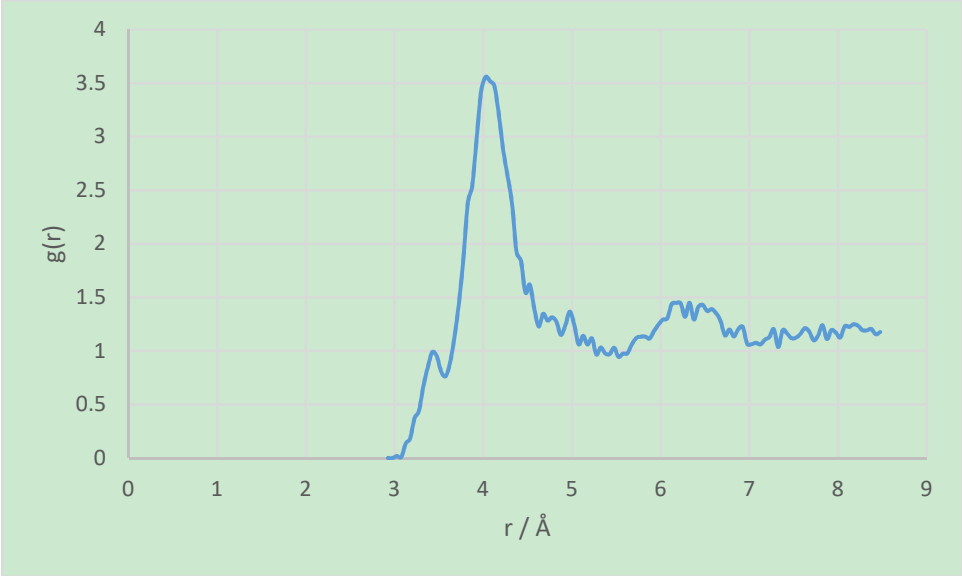

Figure S29. U-Ow RDF for $UO_2(OH)_4^{2-}$ on the (001) surface of portlandite.

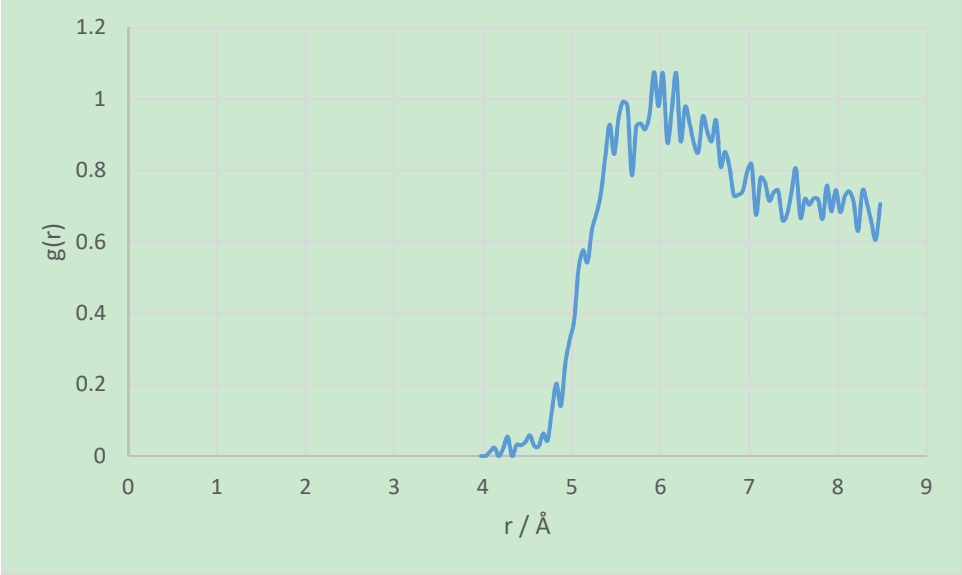

Figure S30. U-Ca RDF for $UO_2(OH)_4^{2-}$ on the (001) surface of portlandite.

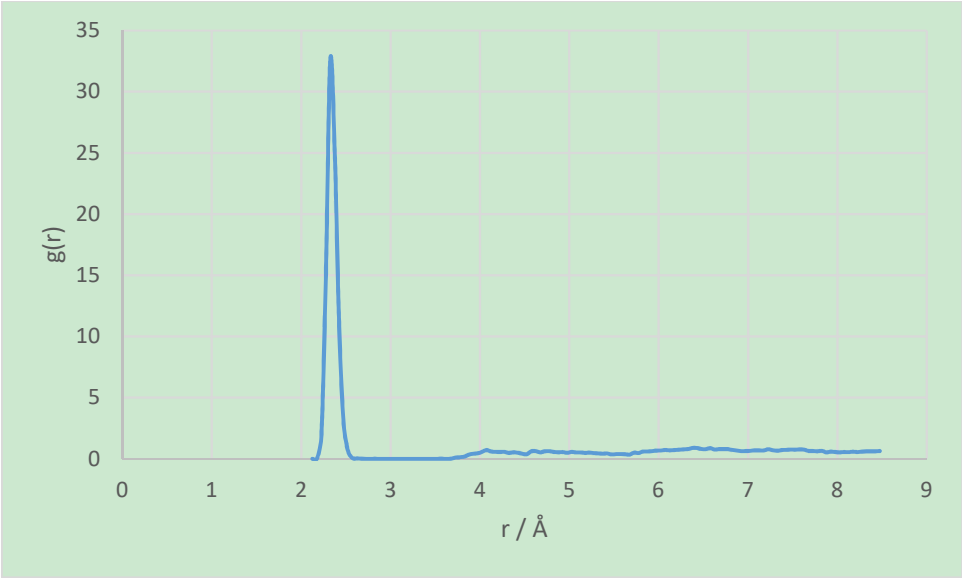

Figure S31. U-Oh RDF for $UO_2(OH)_5^{3-}$ on the (001) surface of portlandite.

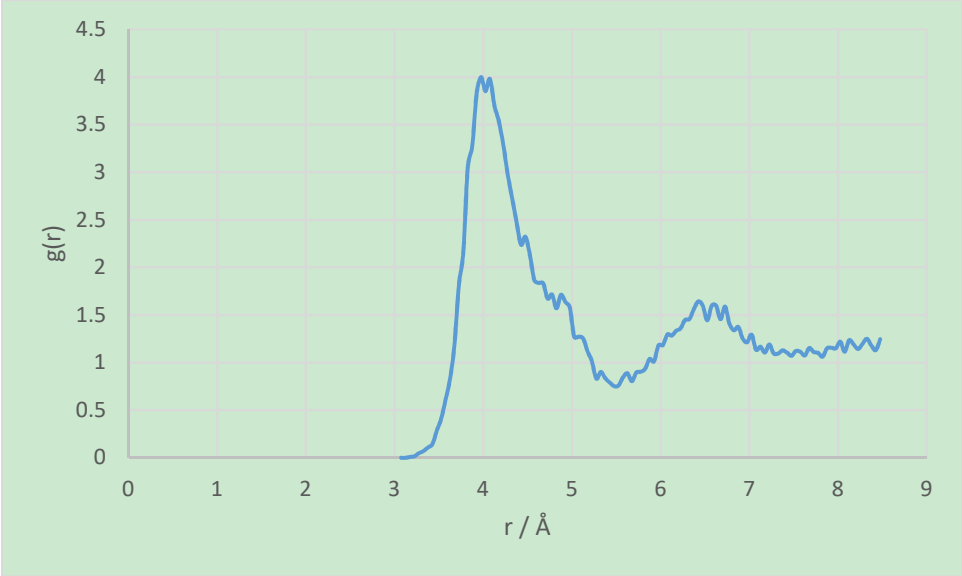

Figure S32. U-Ow RDF for $UO_2(OH)_5^{3-}$ on the (001) surface of portlandite.

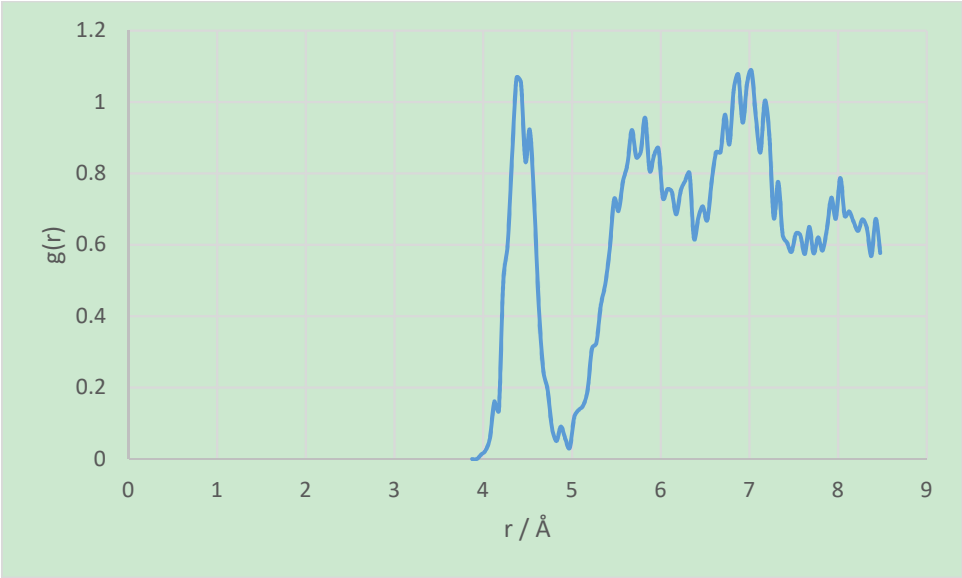

Figure S33. U-Ca RDF for $UO_2(OH)_5^{3-}$ on the (001) surface of portlandite.

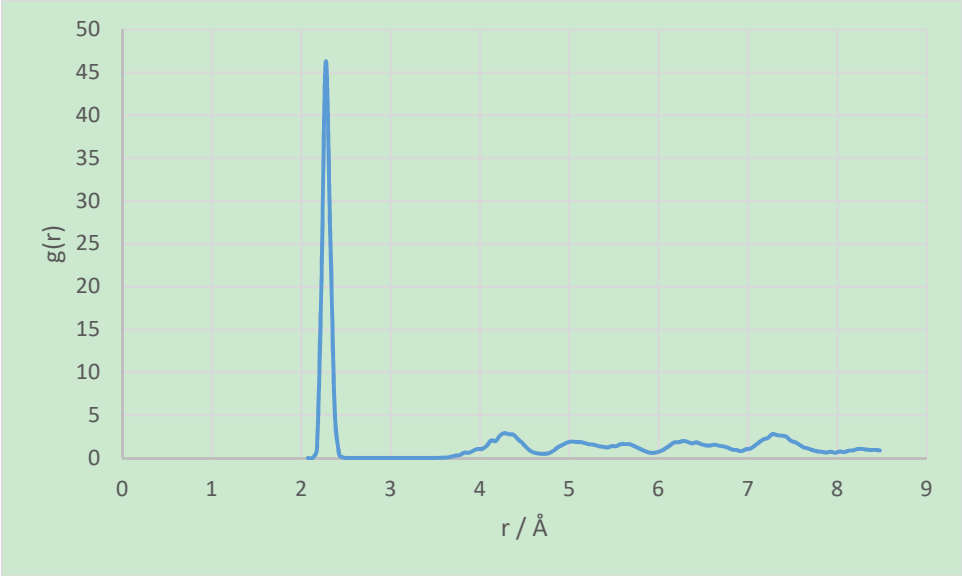

Figure S34. U-Oh RDF for UO_2^{2+} on the (100) surface of portlandite.

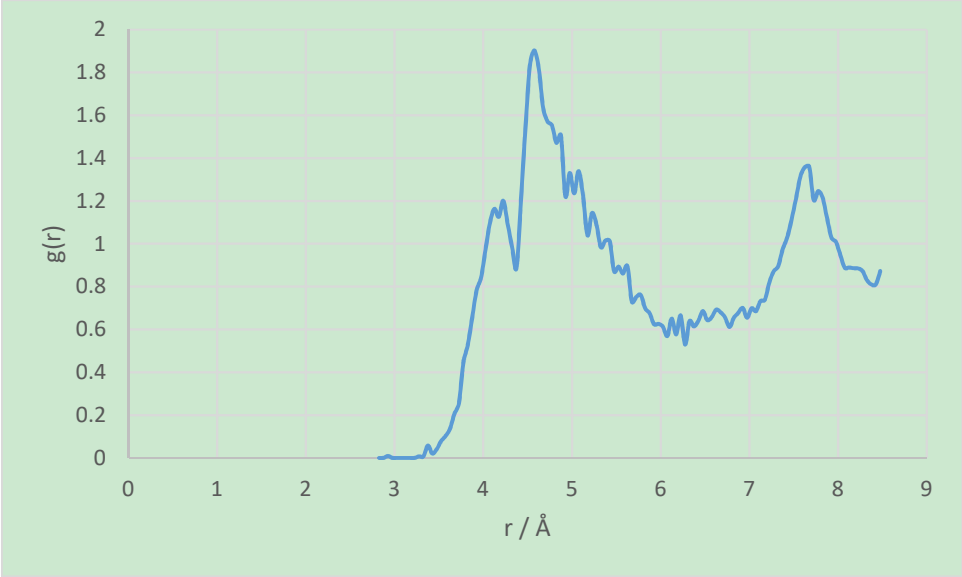

Figure S35. U-Ow RDF for UO_2^{2+} on the (100) surface of portlandite.

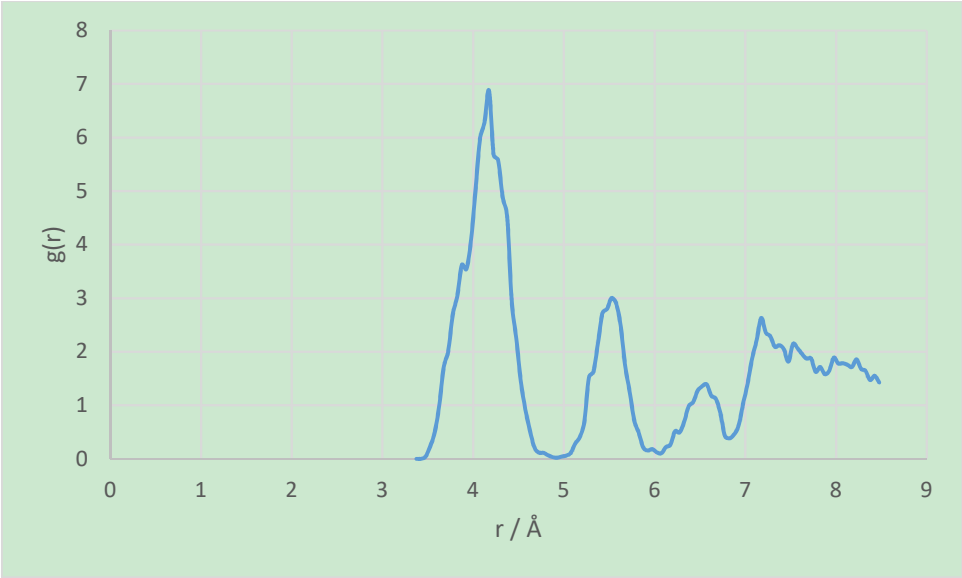

Figure S36. U-Ca RDF for UO_2^{2+} on the (100) surface of portlandite.

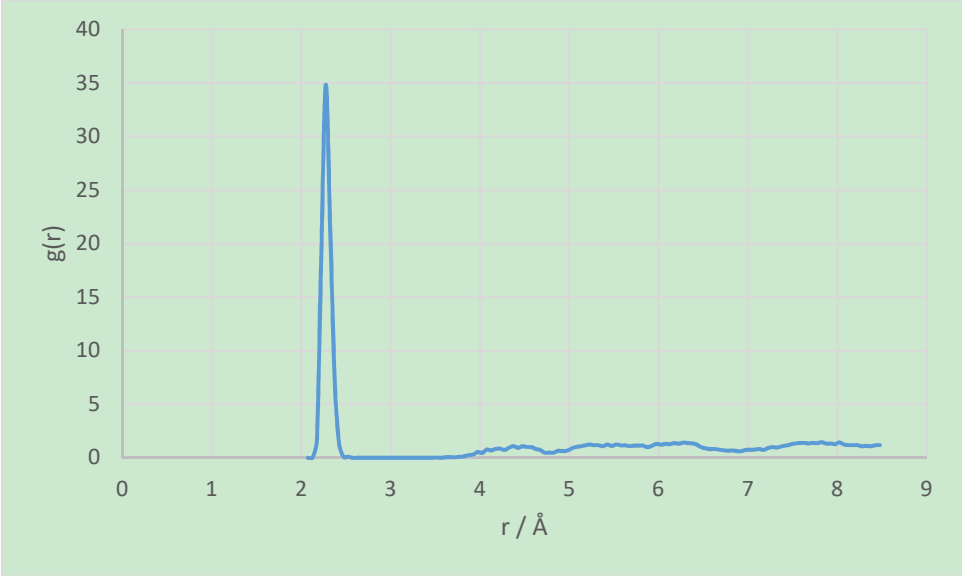

Figure S37. U-Oh RDF for $UO_2(OH)^+$ on the (100) surface of portlandite.

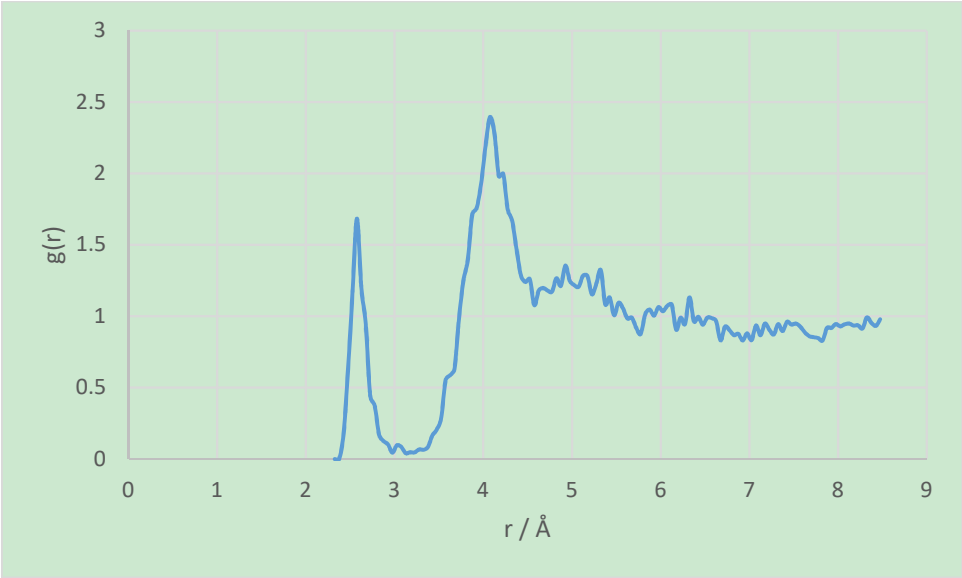

Figure S38. U-Ow RDF for $UO_2(OH)^+$ on the (100) surface of portlandite.

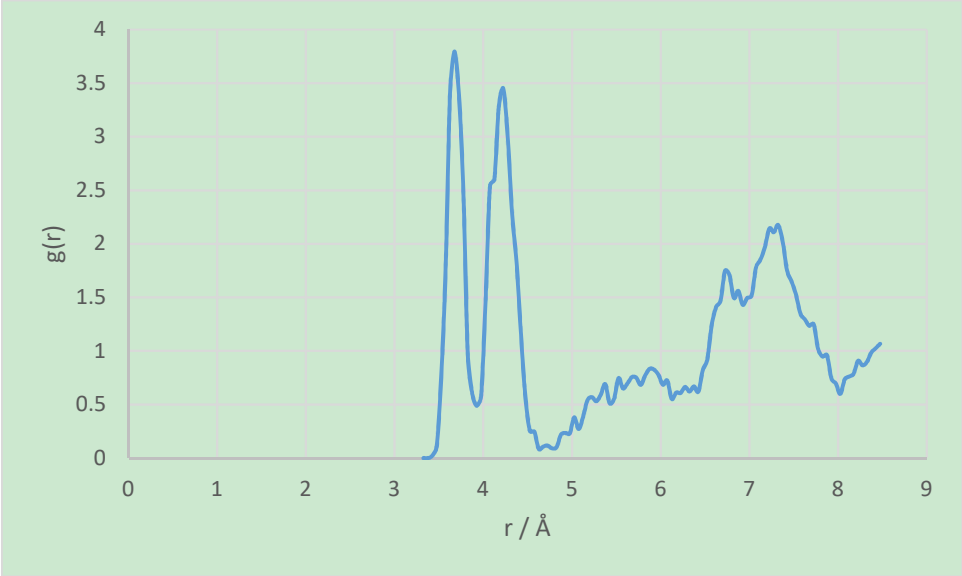

Figure S39. U-Ca RDF for $UO_2(OH)^+$ on the (100) surface of portlandite.

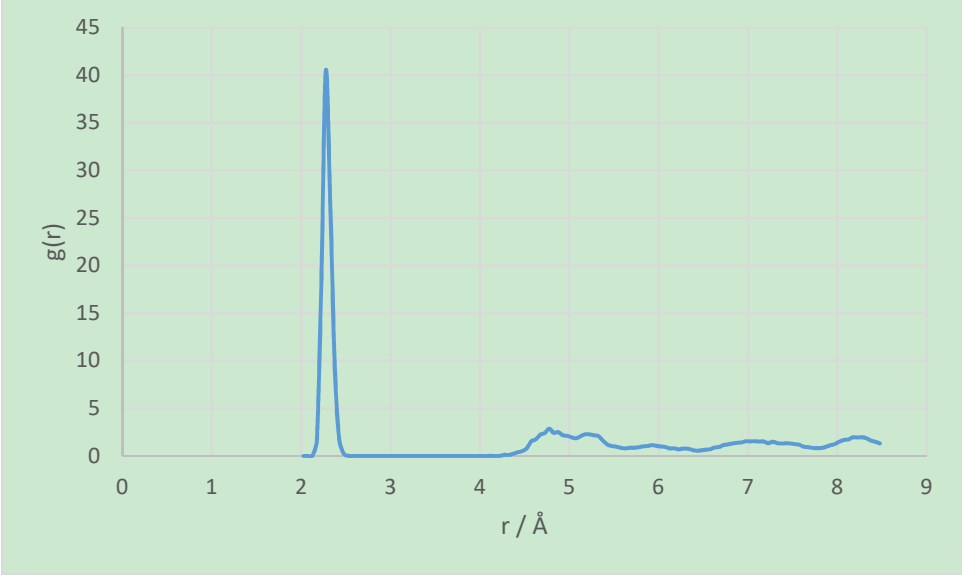

Figure S40. U-Oh RDF for $UO_2(OH)_2$ on the (100) surface of portlandite.

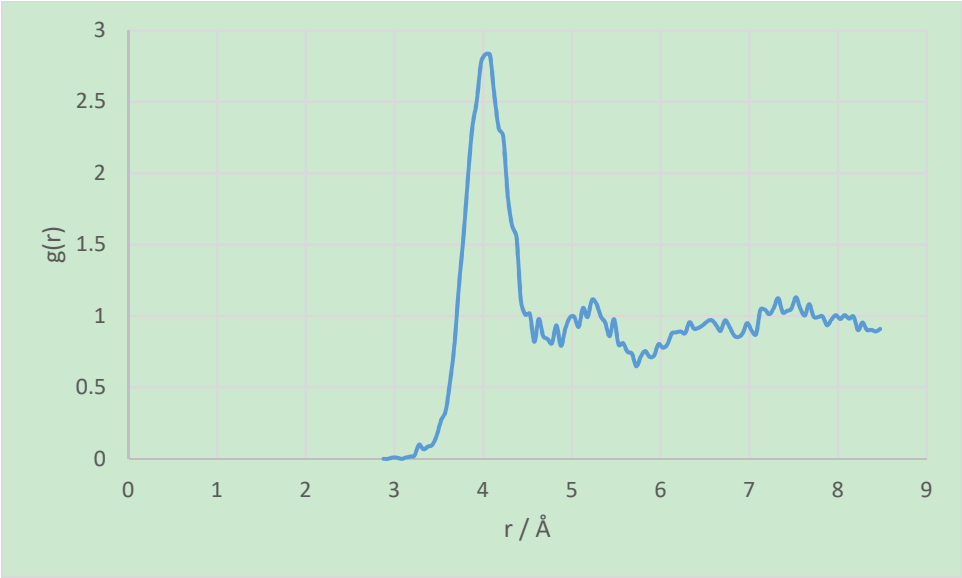

Figure S41. U-Ow RDF for $UO_2(OH)_2$ on the (100) surface of portlandite.

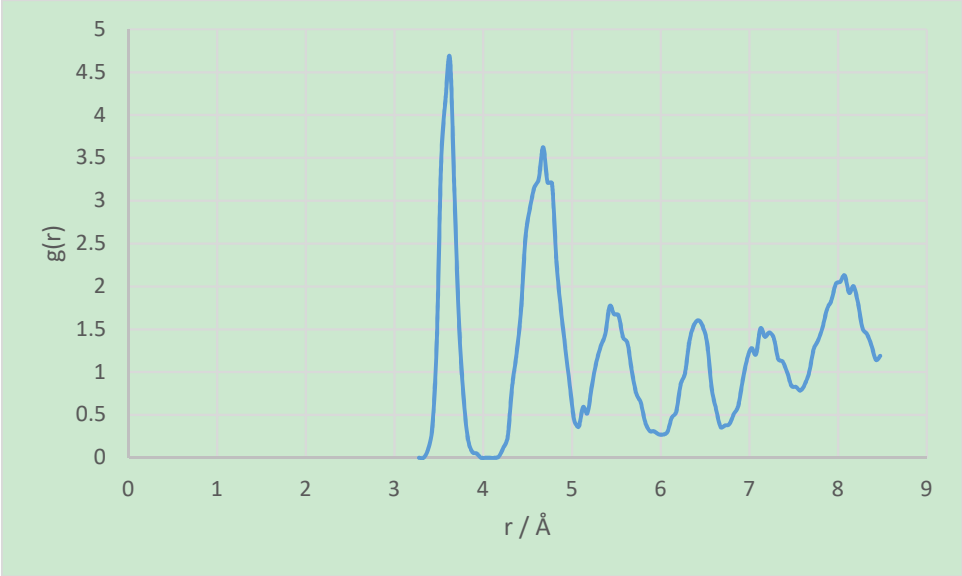

Figure S42. U-Ca RDF for $UO_2(OH)_2$ on the (100) surface of portlandite.

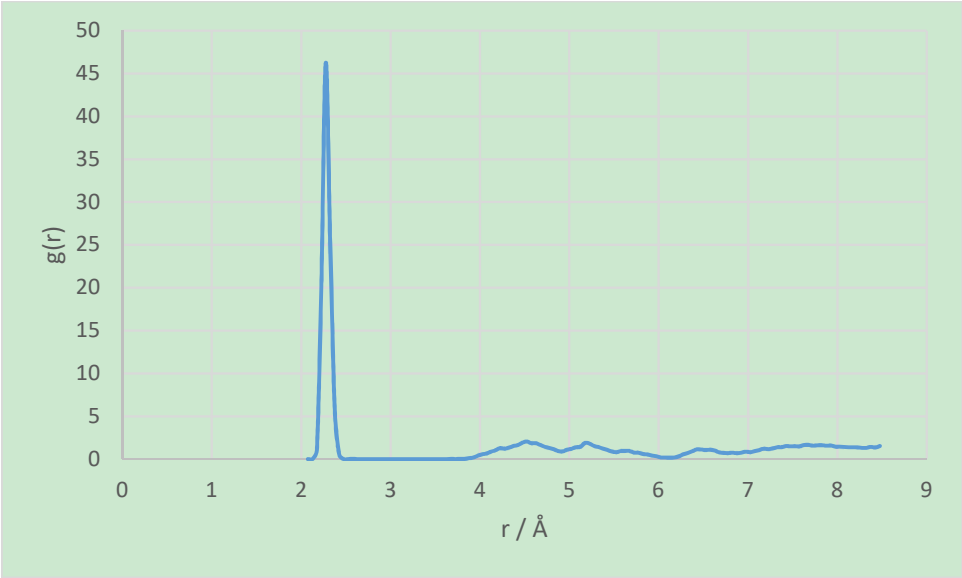

Figure S43. U-Oh RDF for $UO_2(OH)_3^-$ on the (100) surface of portlandite.

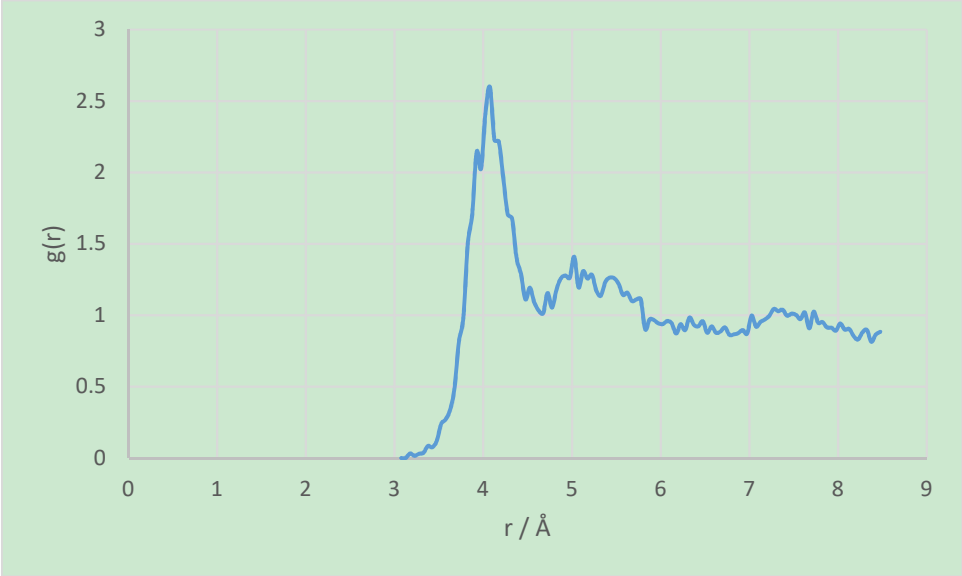

Figure S44. U-Ow RDF for $UO_2(OH)_3^-$ on the (100) surface of portlandite.

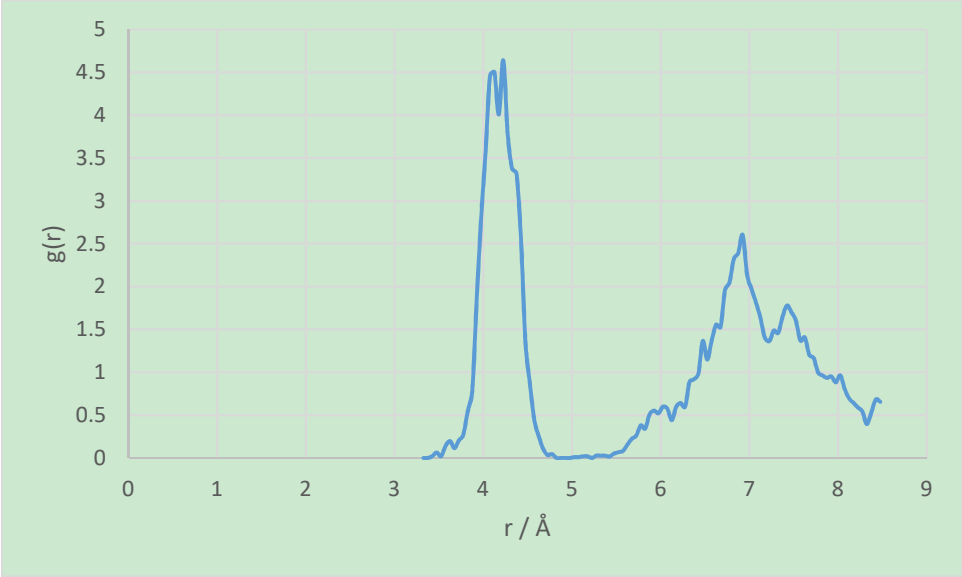

Figure S45. U-Ca RDF for $UO_2(OH)_3^-$ on the (100) surface of portlandite.

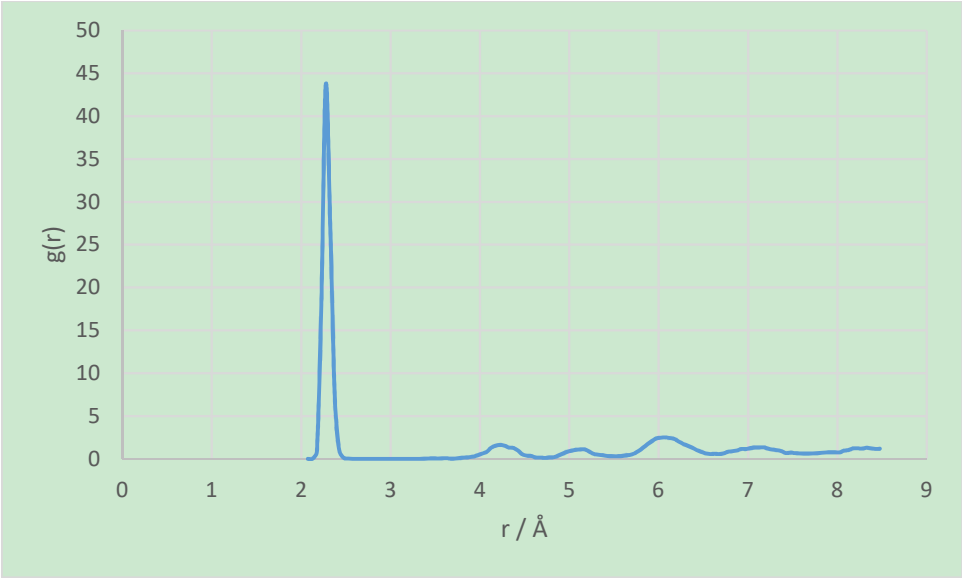

Figure S46. U-Oh RDF for $UO_2(OH)_4^{2-}$ on the (100) surface of portlandite.

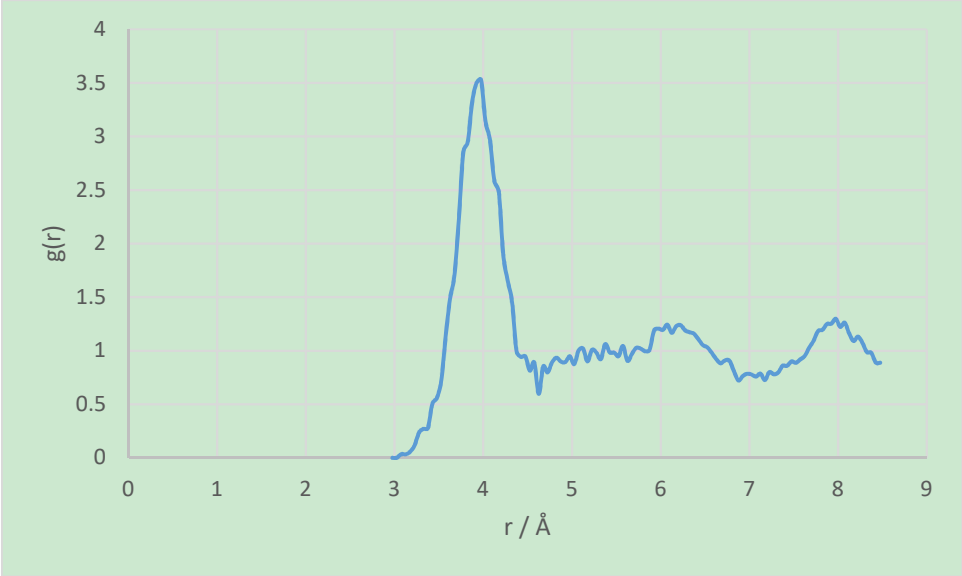

Figure S47. U-Ow RDF for $UO_2(OH)_4^{2-}$ on the (100) surface of portlandite.

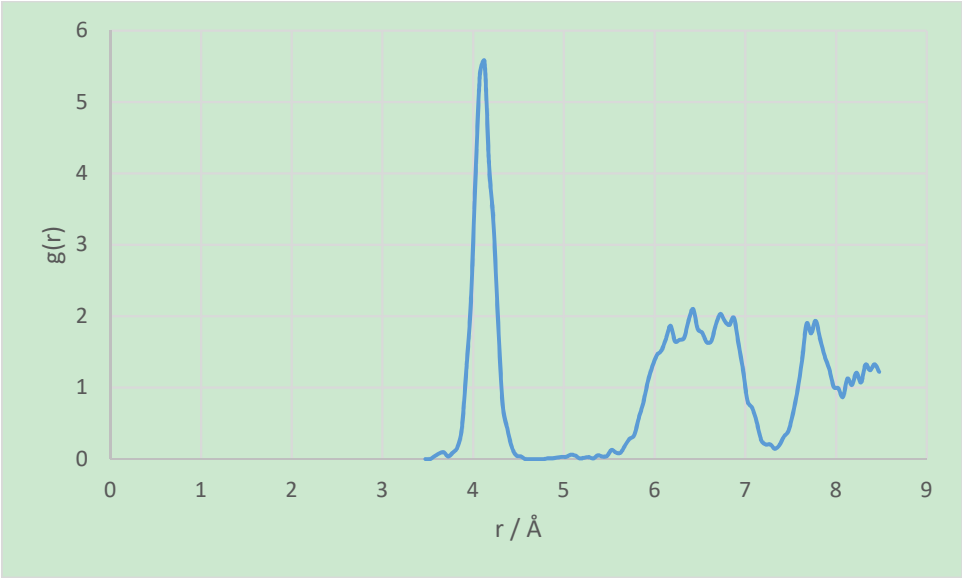

Figure S48. U-Ca RDF for $UO_2(OH)_4^{2-}$ on the (100) surface of portlandite.

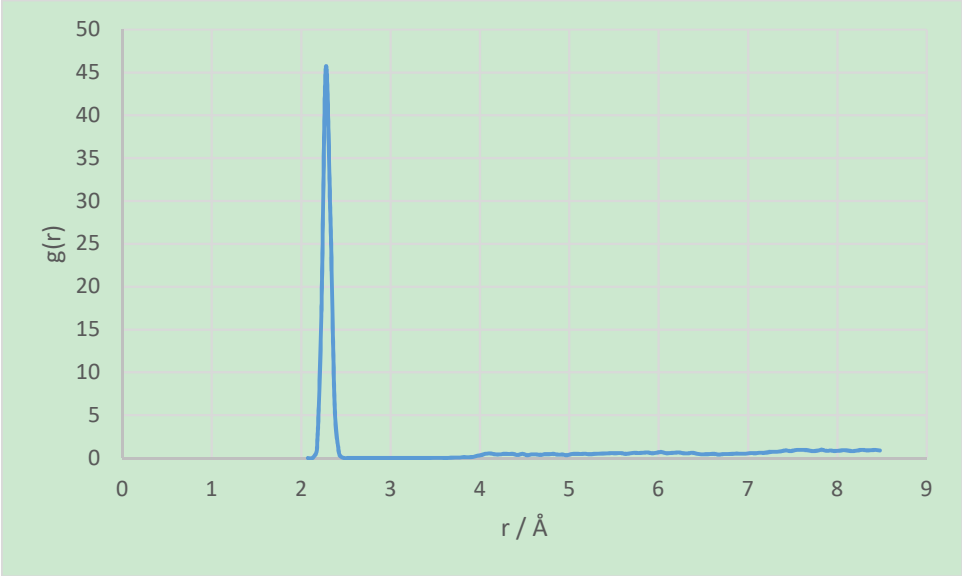

Figure S49. U-Oh RDF for $UO_2(OH)_5^{3-}$ on the (100) surface of portlandite.

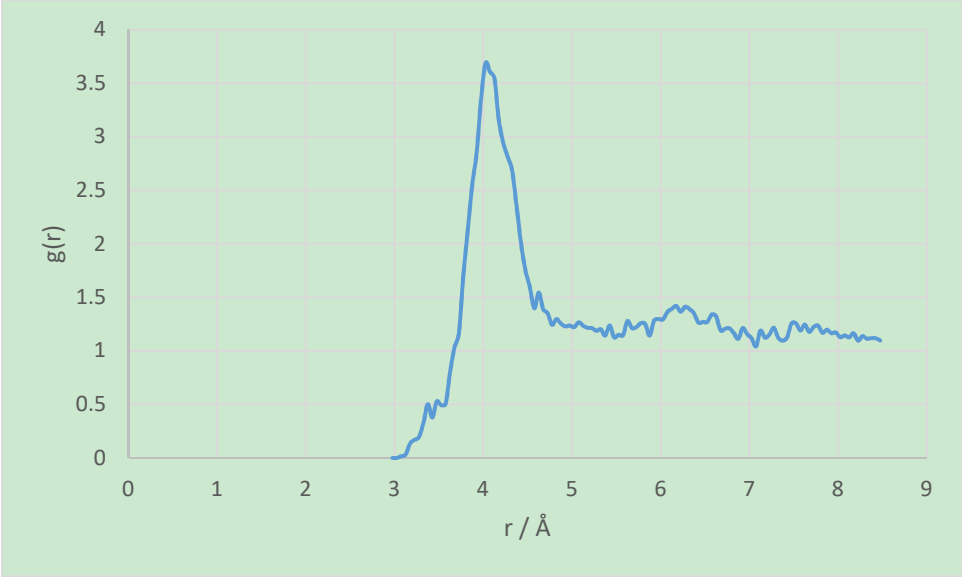

Figure S50. U-Ow RDF for $UO_2(OH)_5^{3-}$ on the (100) surface of portlandite.

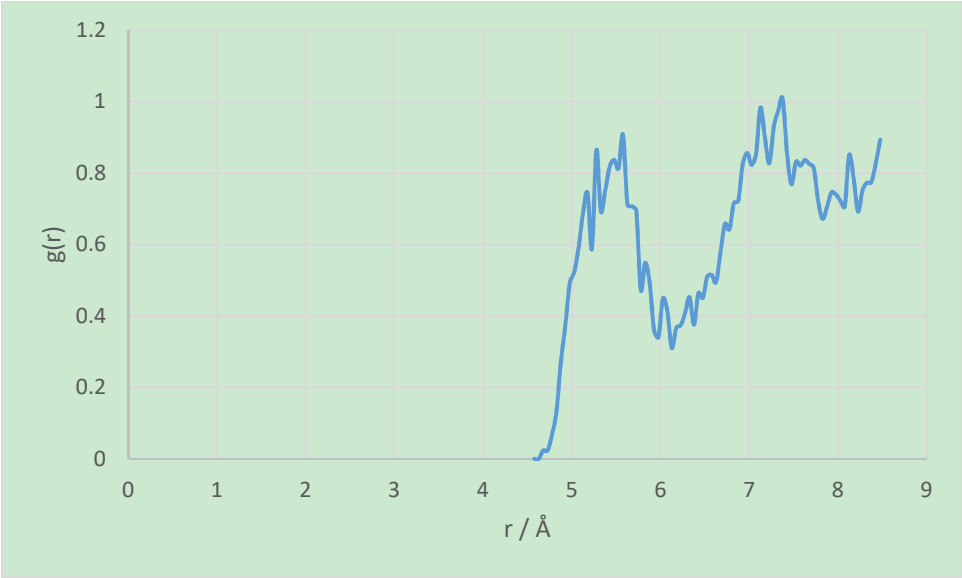

Figure S51. U-Ca RDF for $UO_2(OH)_5^{3-}$ on the (100) surface of portlandite.

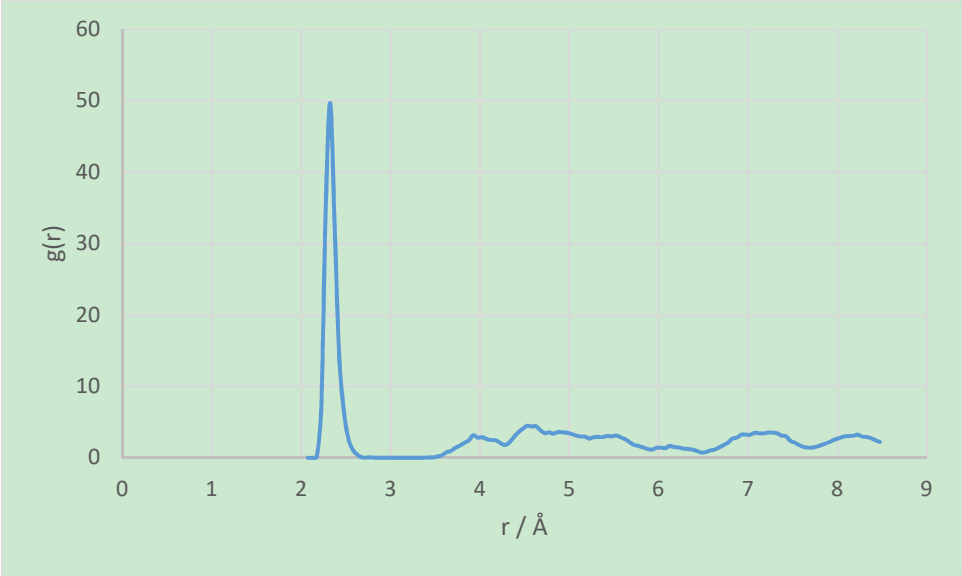

Figure S52. U-Oh RDF for UO_2^{2+} on the (203) surface of portlandite.

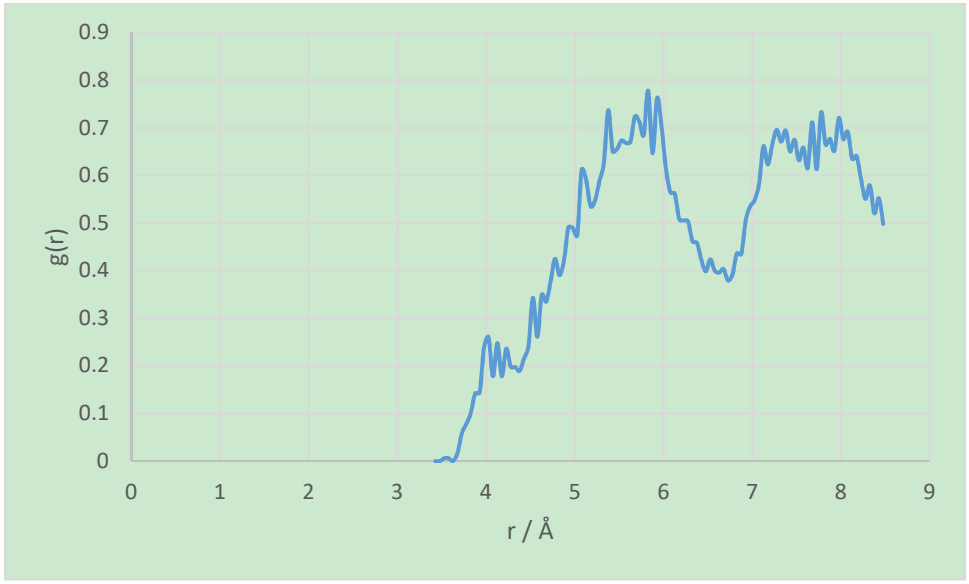

Figure S53. U-Ow RDF for UO_2^{2+} on the (203) surface of portlandite.

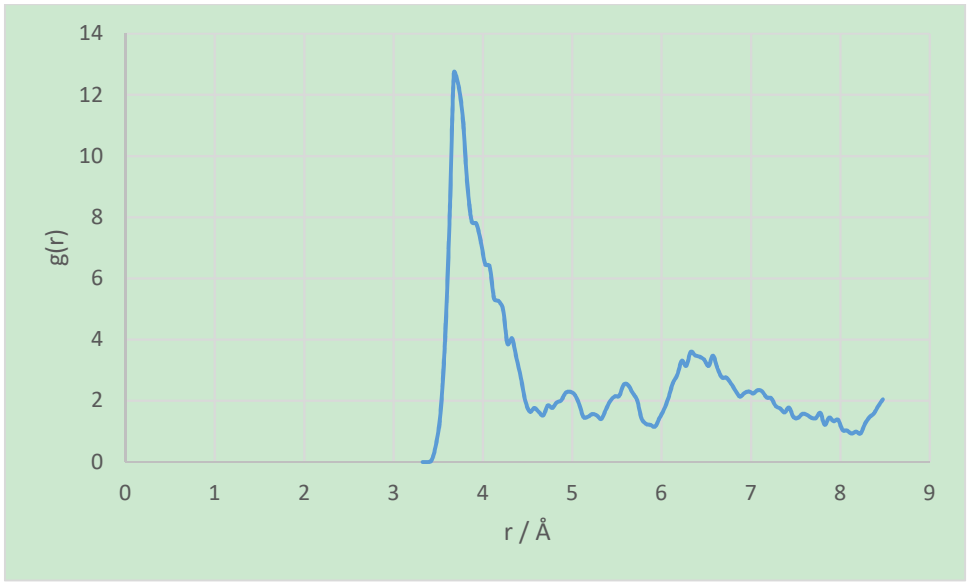

Figure S54. U-Ca RDF for UO_2^{2+} on the (203) surface of portlandite.

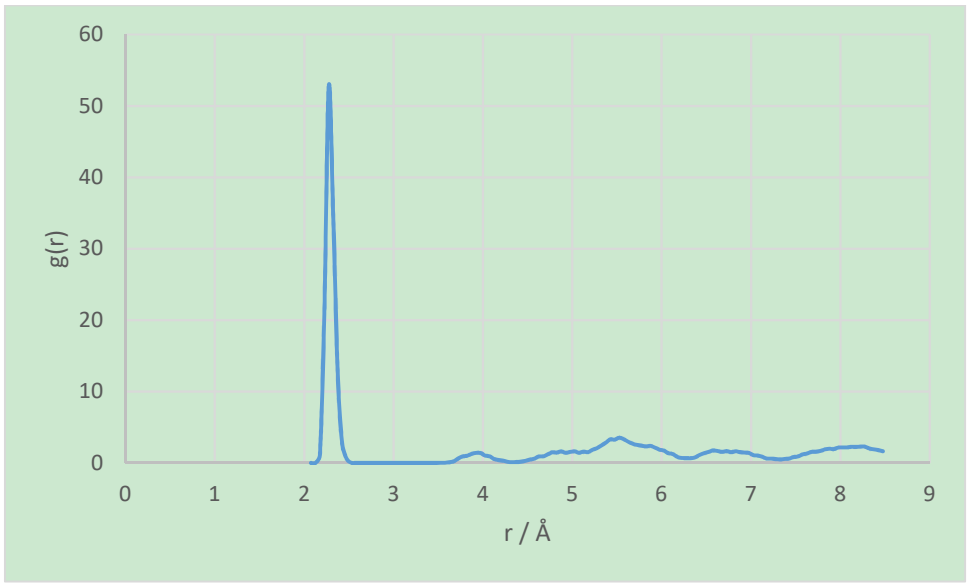

Figure S55. U-Oh RDF for $UO_2(OH)^+$ on the (203) surface of portlandite.

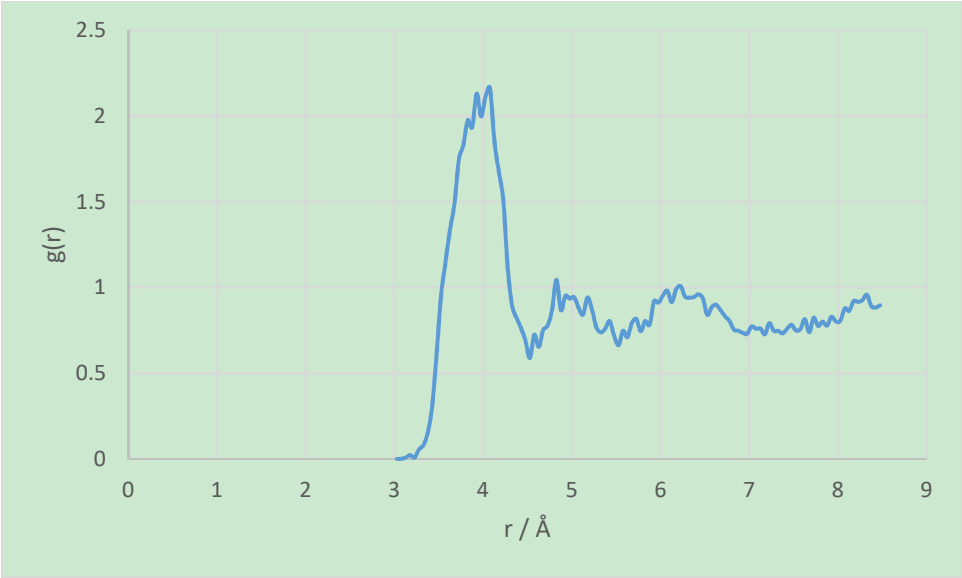

Figure S56. U-Ow RDF for $UO_2(OH)^+$ on the (203) surface of portlandite.

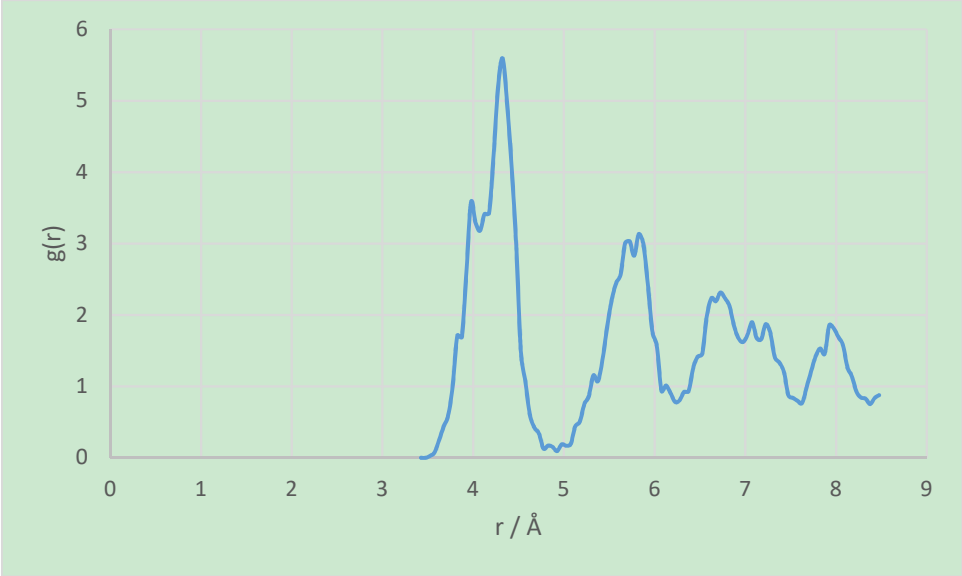

Figure S57. U-Ca RDF for $UO_2(OH)^+$ on the (203) surface of portlandite.

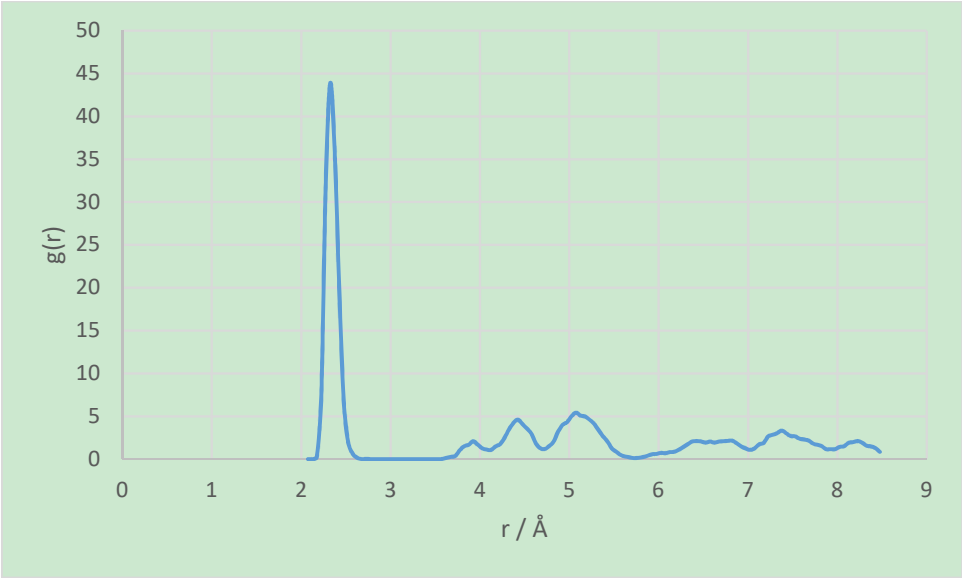

Figure S58. U-Oh RDF for $UO_2(OH)_2$ on the (203) surface of portlandite.

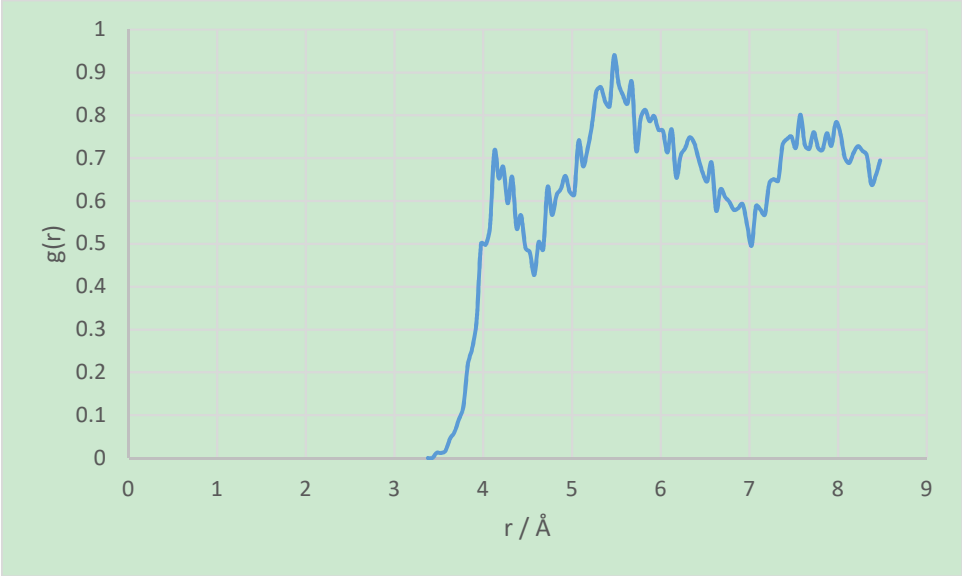

Figure S59. U-Ow RDF for $UO_2(OH)_2$ on the (203) surface of portlandite.

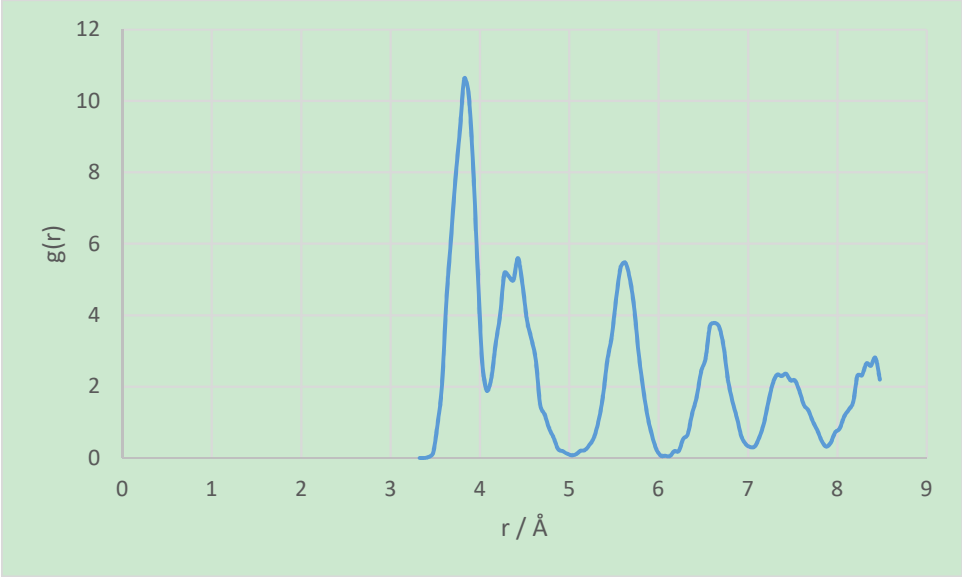

Figure S60. U-Ca RDF for $UO_2(OH)_2$ on the (203) surface of portlandite.

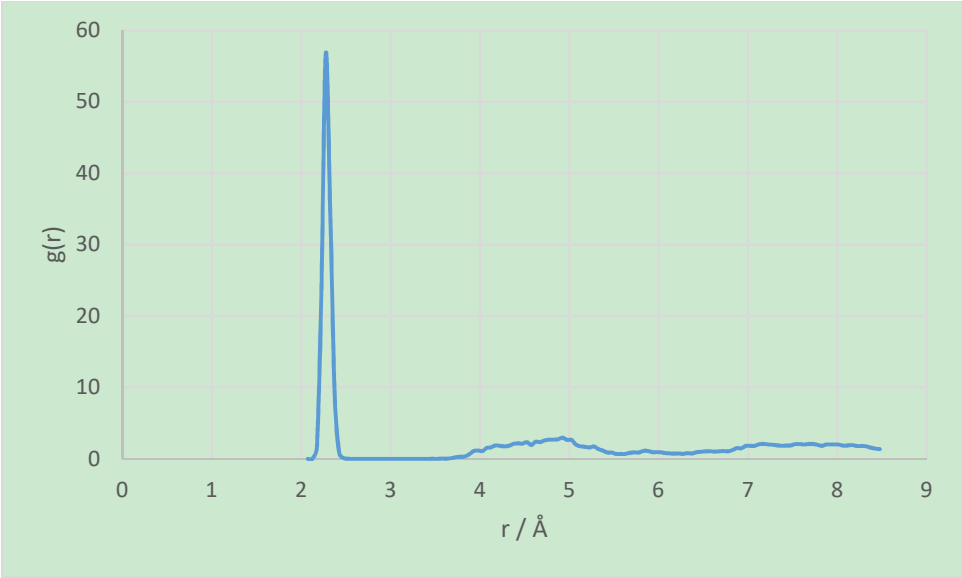

Figure S61. U-Oh RDF for $UO_2(OH)_3^-$ on the (203) surface of portlandite.

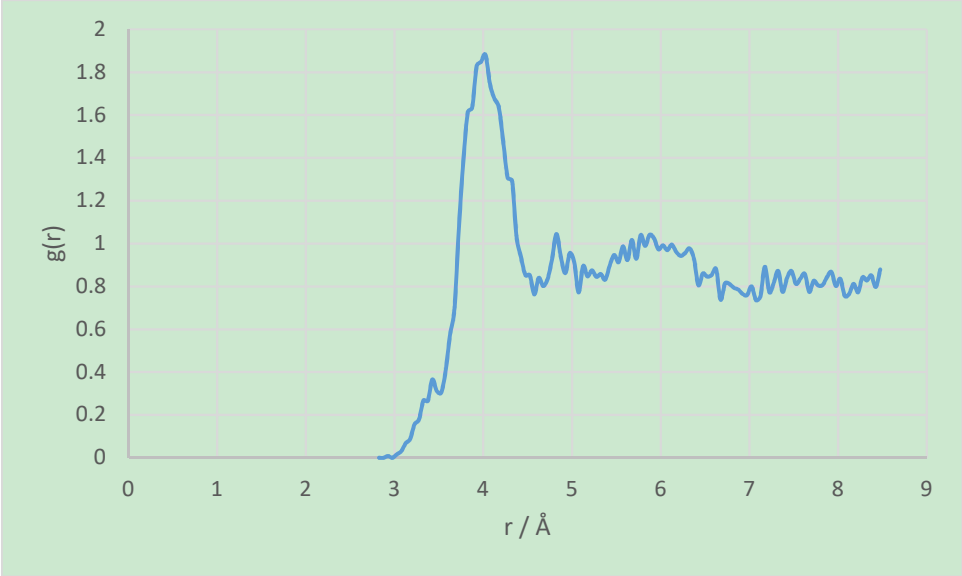

Figure S62. U-Ow RDF for $UO_2(OH)_3^-$ on the (203) surface of portlandite.

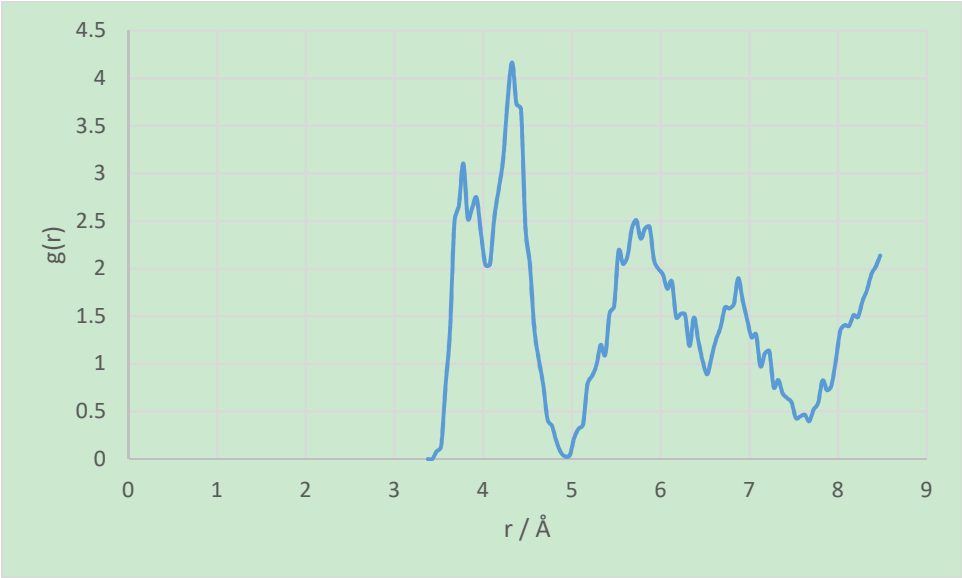

Figure S63. U-Ca RDF for $UO_2(OH)_3^-$ on the (203) surface of portlandite.

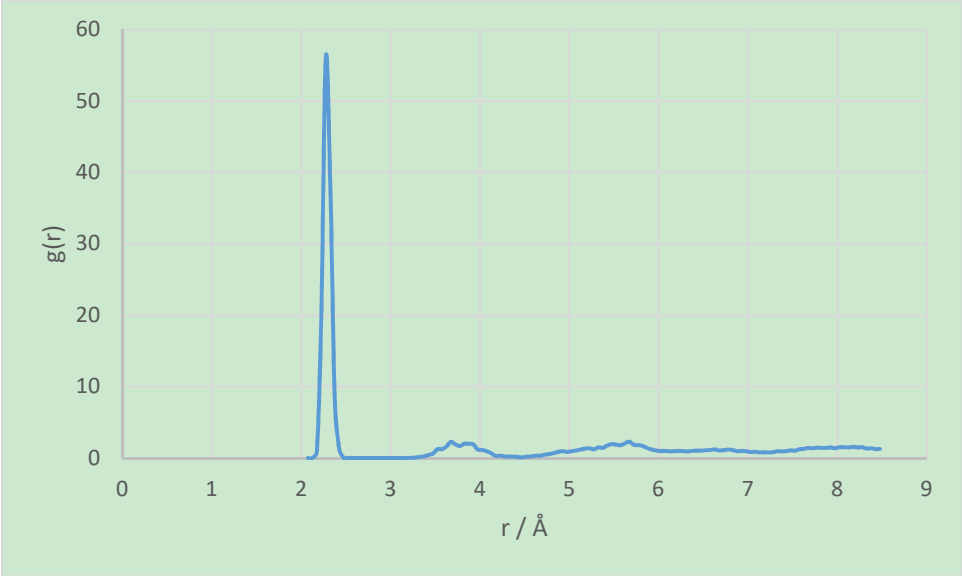

Figure S64. U-Oh RDF for $UO_2(OH)_4^{2-}$ on the (203) surface of portlandite.

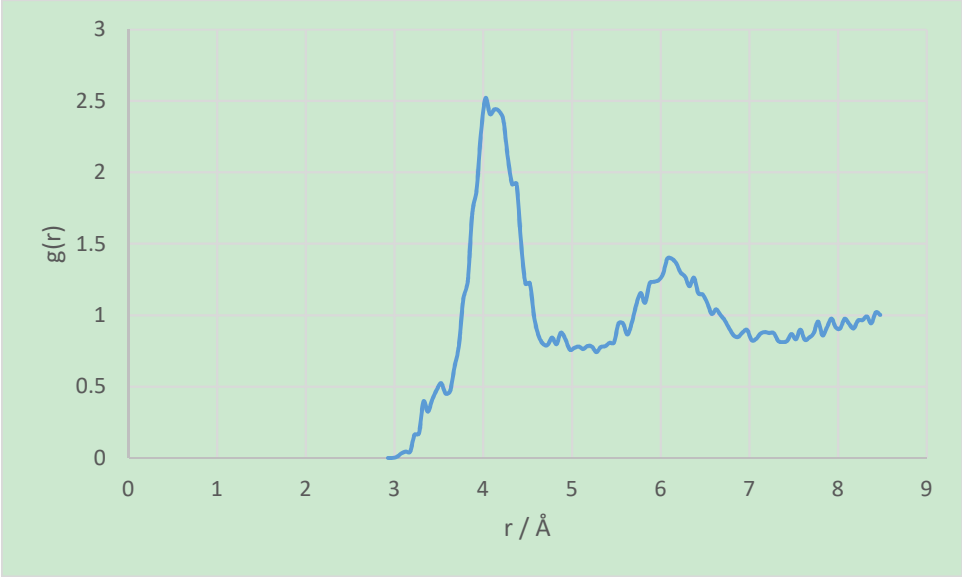

Figure S65. U-Ow RDF for $UO_2(OH)_4^{2-}$ on the (203) surface of portlandite.

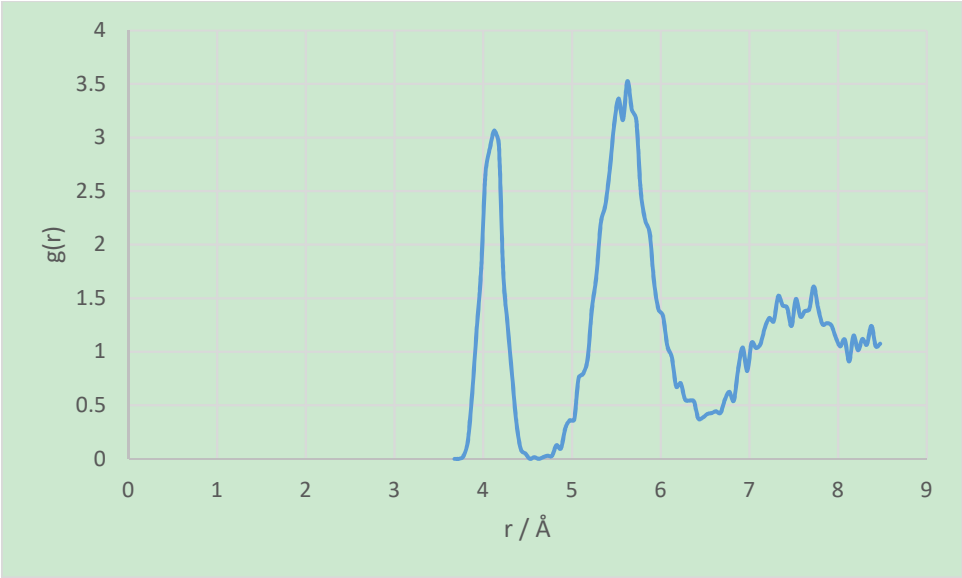

Figure S66. U-Ca RDF for $UO_2(OH)_4^{2-}$ on the (203) surface of portlandite.

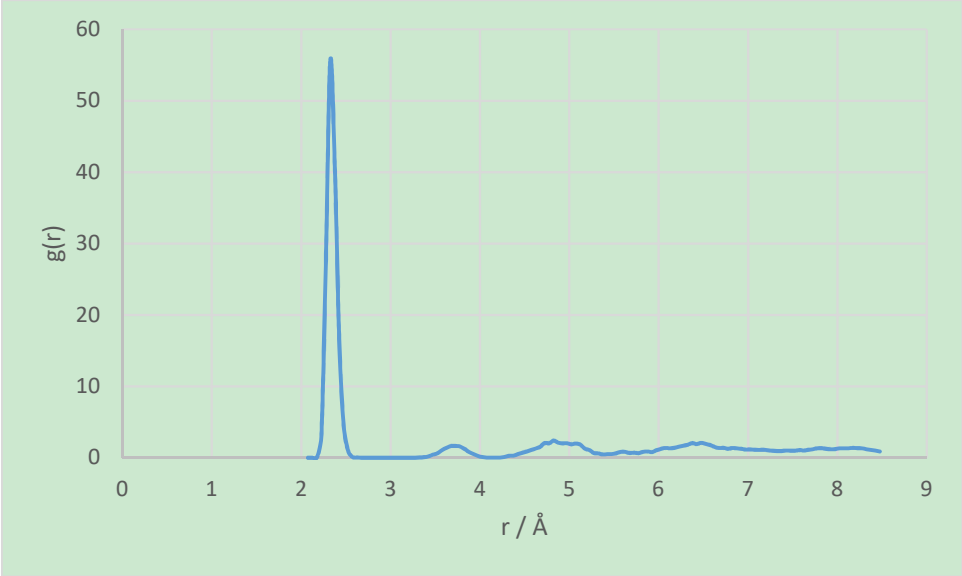

Figure S67. U-Oh RDF for $UO_2(OH)_5^{3-}$ on the (203) surface of portlandite.

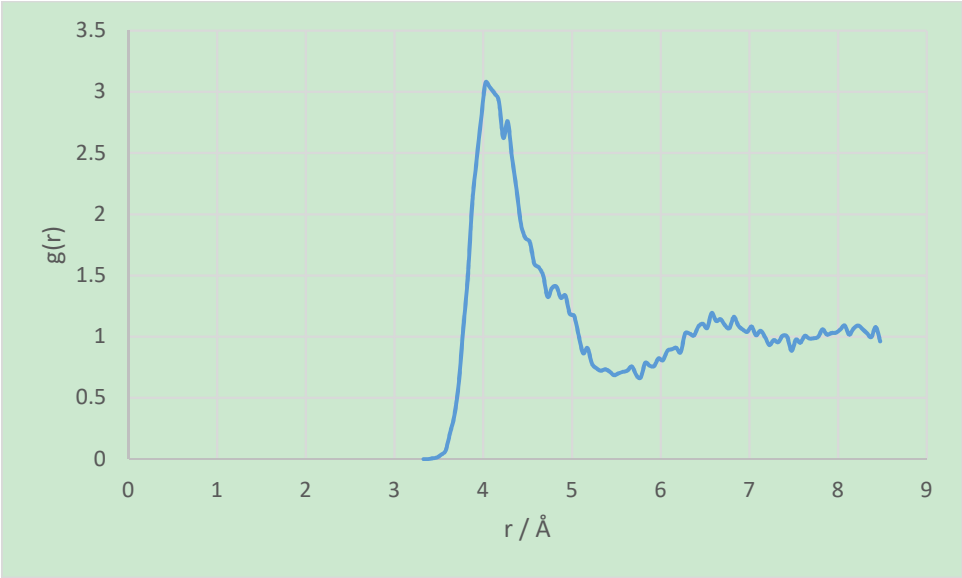

Figure S68. U-Ow RDF for $UO_2(OH)_5^{3-}$ on the (203) surface of portlandite.

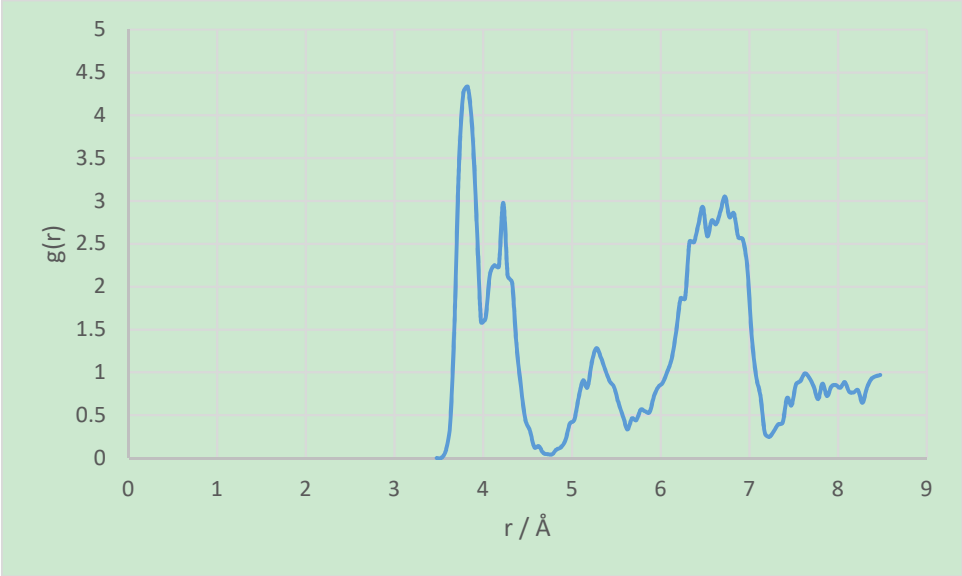

Figure S69. U-Ca RDF for $UO_2(OH)_5^{3-}$ on the (203) surface of portlandite.

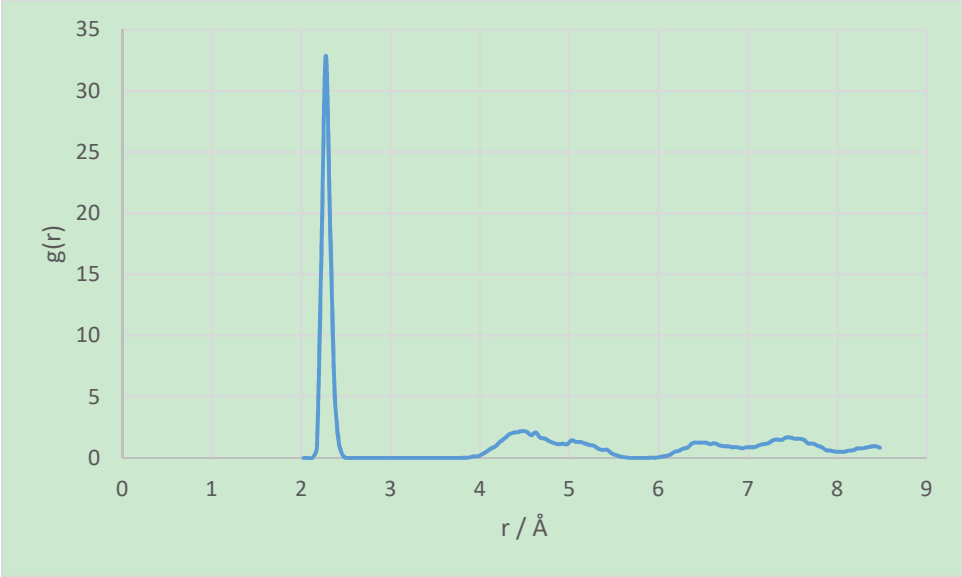

Figure S70. U-Oh RDF for $UO_2(OH)_4^{2-}$ on the (001-OH) surface of portlandite.

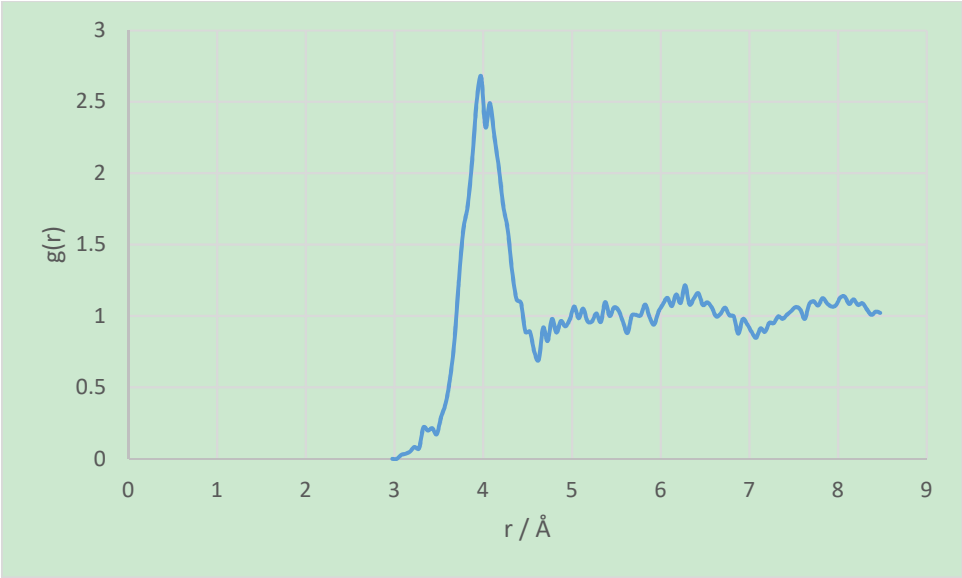

Figure S71. U-Ow RDF for $UO_2(OH)_4^{2-}$ on the (001-OH) surface of portlandite.

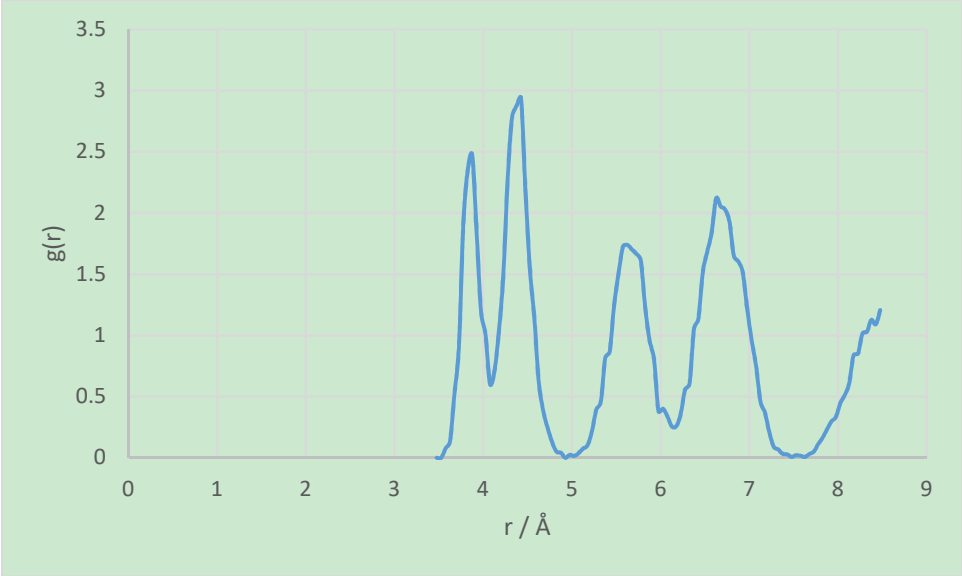

Figure S72. U-Ca RDF for $UO_2(OH)_4^{2-}$ on the (001-OH) surface of portlandite.

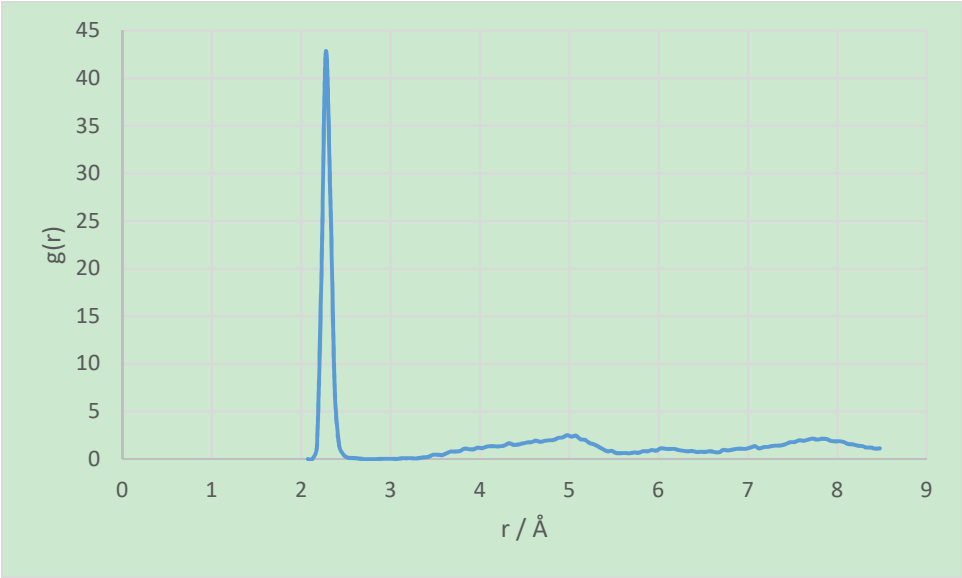

Figure S73. U-Oh RDF for $UO_2(OH)_4^{2-}$ on the (100-OH) surface of portlandite.

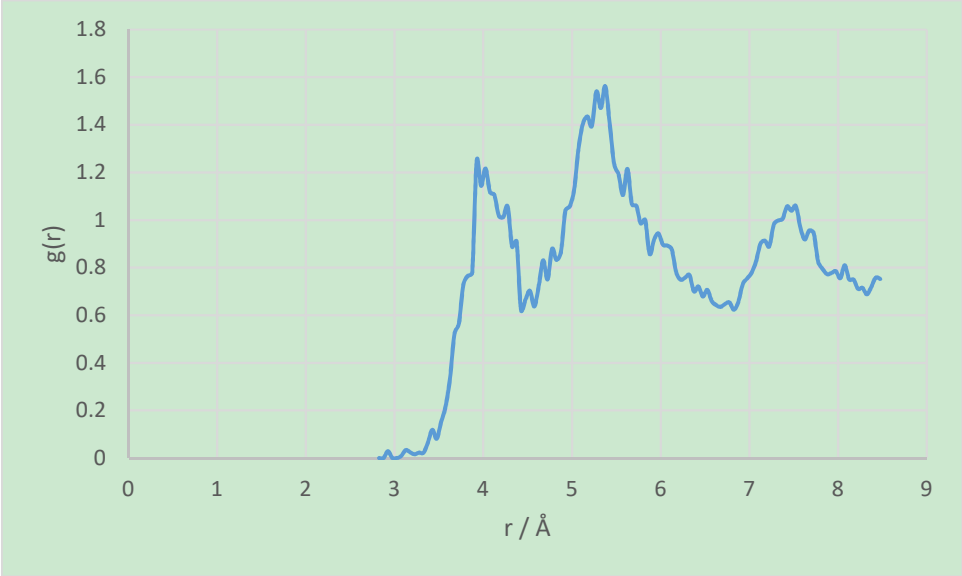

Figure S74. U-Ow RDF for $UO_2(OH)_4^{2-}$ on the (100-OH) surface of portlandite.

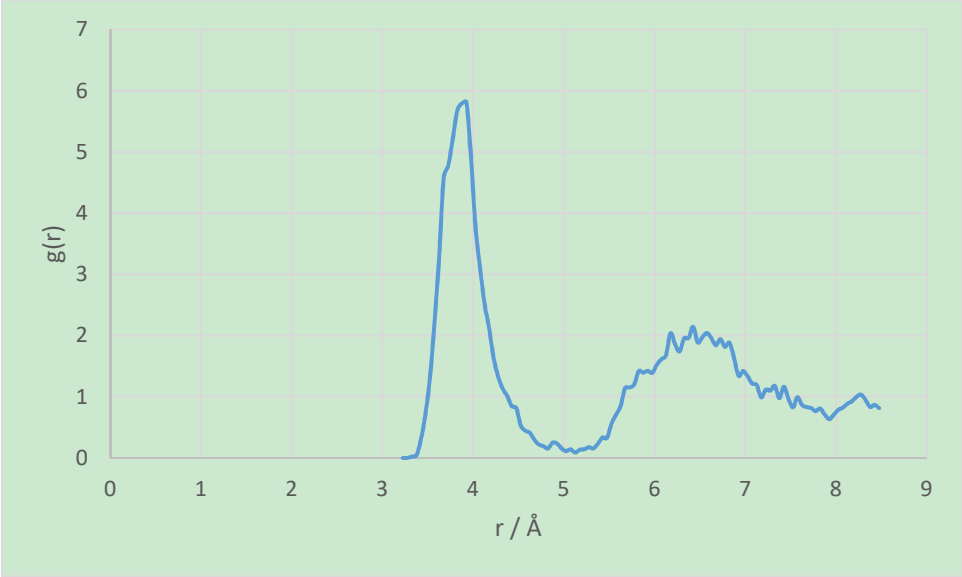

Figure S75. U-Ca RDF for $UO_2(OH)_4^{2-}$ on the (100-OH) surface of portlandite.

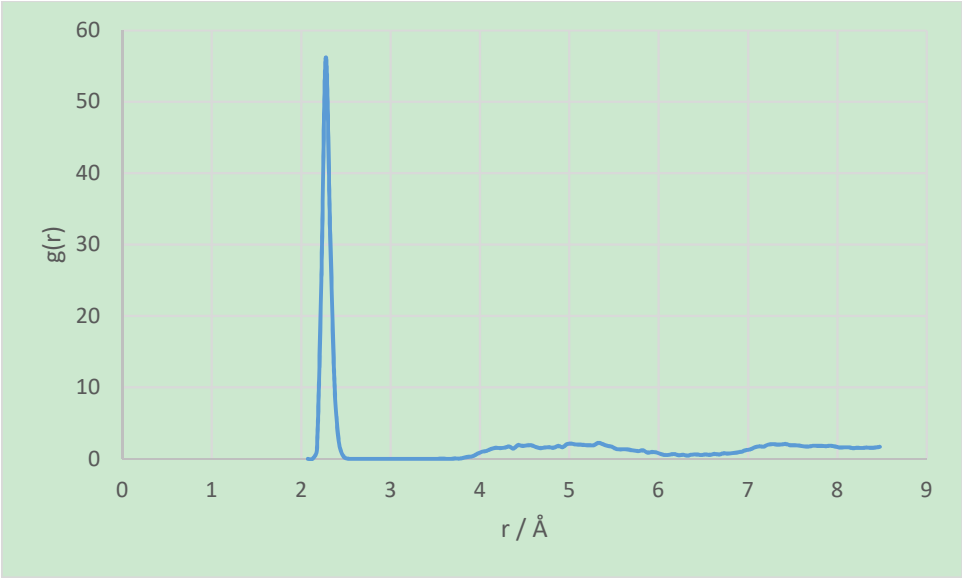

Figure S76. U-Oh RDF for $UO_2(OH)_4^{2-}$ on the (203-OH) surface of portlandite.

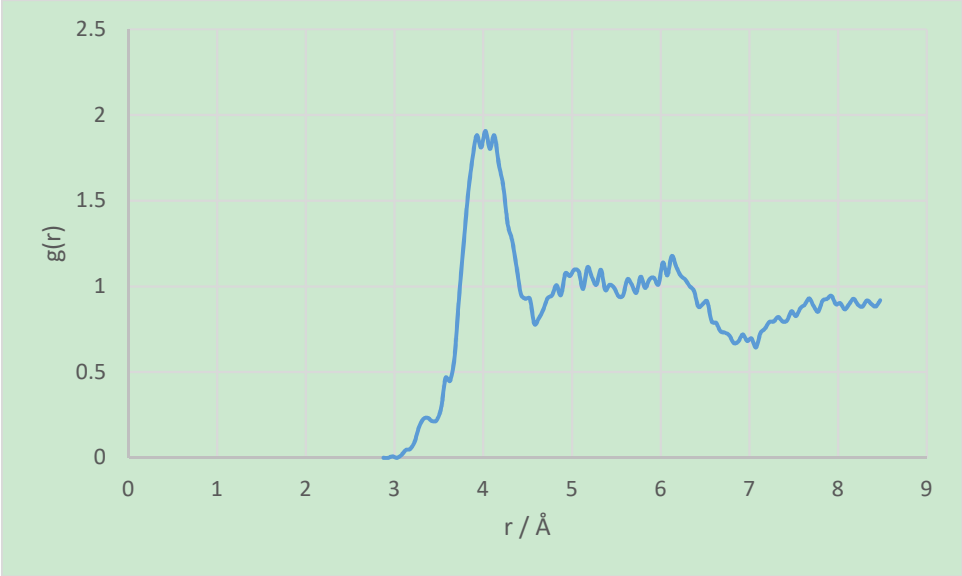

Figure S77. U-Ow RDF for $UO_2(OH)_4^{2-}$ on the (203-OH) surface of portlandite.

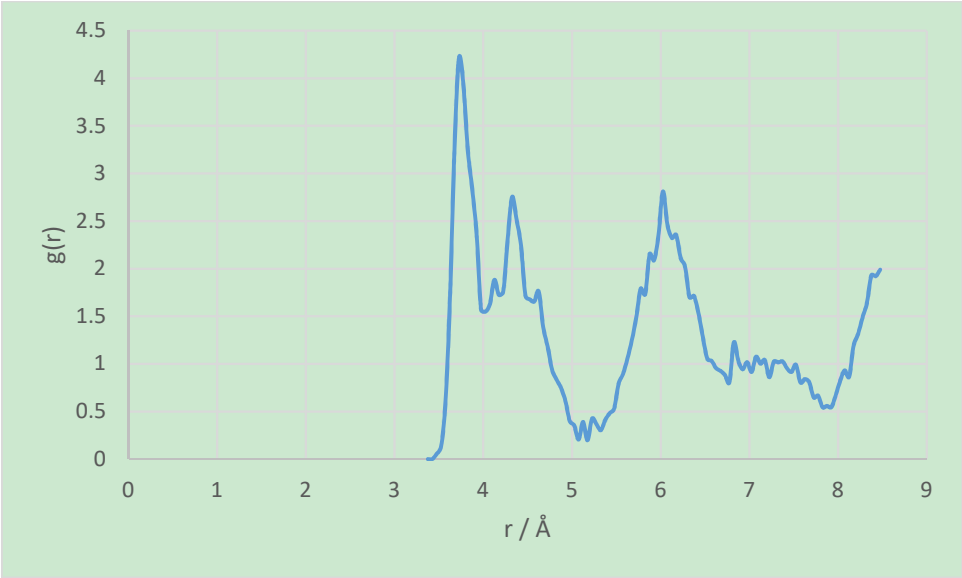

Figure S78. U-Ca RDF for $UO_2(OH)_4^{2-}$ on the (203-OH) surface of portlandite.